

Linköping studies in science and technology. Dissertation No. 1426

Spin Properties in InAs/GaAs Quantum Dot based Nanostructures

Jan Beyer



Linköping University
INSTITUTE OF TECHNOLOGY

Functional Electronic Materials Division
Department of Physics, Chemistry and Biology
Linköping university, Sweden

Linköping 2012

Copyright © Jan Beyer 2012
unless otherwise stated

ISBN: 978-91-7519-965-8
ISSN: 0345-7524

The front cover shows atomic force microscopy graphs for three of the samples that were studied in this thesis. The back cover shows an illustration of the process of non-resonant optical orientation of an electron-hole pair with subsequent polarized trion recombination in a quantum dot.

Printed by LiU-Tryck, Linköping, Sweden 2012

Semiconductor quantum dots (QDs) are a promising building block of future spin-functional devices for applications in spintronics and quantum information processing. Essential to the realization of such devices is our ability to create a desired spin orientation of charge carriers (electrons and holes), typically via injection of spin polarized carriers from other parts of the QD structures. In this thesis, the optical orientation technique has been used to characterize spin generation, relaxation and detection in self-assembled single and multi-QD structures in the InAs/GaAs system prepared by modern molecular beam epitaxy technique.

Optical generation of spin-oriented carriers in the wetting layer (WL) and GaAs barrier was carried out via circularly polarized excitation of uncorrelated electron-hole pairs from band-to-band transitions or via resonant excitation of correlated electron-hole pairs, i.e. excitons. It was shown that the generation and injection of uncorrelated electron-hole pairs is advantageous for spin-preserving injection into the QDs. The lower spin injection efficiency of excitons was attributed to an enhanced spin relaxation caused by the mutual electron-hole Coulomb exchange interaction. This correlation affects the spin injection efficiency up to elevated temperatures of around 150 K.

Optical orientation at the energy of the WL light-hole (lh) exciton (XL) is accompanied by simultaneous excitation from the heavy-hole (hh) valence band at high \vec{k} -vectors. Quantum interference of the two excitation pathways in the spectral vicinity of the XL energy resulted in occurrence of an asymmetric absorption peak, a Fano resonance. Complete quenching of spin generation efficiency at the resonance was observed and attributed to enhanced spin scattering between the hh and lh valence bands in conjunction with the Coulomb exchange interaction in the XL. This mechanism remains effective up to temperatures exceeding 100 K.

In longitudinal magnetic fields up to 2 T, the spin detection efficiency in the QD ensemble was observed to increase by a factor of up to 2.5 in the investigated structures. This is due to the suppression of two spin depolarization mechanisms of the QD electron: the hyperfine interaction with the randomly oriented nuclear spins and the anisotropic exchange interaction with the hole. At higher magnetic fields, when these spin depolarization processes are quenched, only anisotropic QD structures (such as double QDs, aligned along a specific crystallographic axis) still exhibit a rather strong field dependence of the QD electron spin polarization under non-resonant excitation. Here, an increased spin relaxation in the spin injector, i.e. the WL or GaAs barrier, is suggested to lead to more efficient thermalization of the spins

to the lower Zeeman-split spin state before capture to the QD.

Finally, the influence of elevated temperatures on the spin properties of the QD structures was studied. The temperature dependence of dynamic nuclear polarization (DNP) of the host lattice atoms in the QDs and its effect on the QD electron spin relaxation and dephasing were investigated for temperatures up to 85 K. An increase in DNP efficiency with temperature was found, accompanied by a decrease in the extent of spin dephasing. Both effects are attributed to an accelerating electron spin relaxation, suggested to be due to phonon-assisted electron-nuclear spin flip-flops driven by the hyperfine interaction. At even higher temperatures, reaching up to room temperature, a surprising, sharp rise in the QD polarization degree has been found. Experiments in a transverse magnetic field showed a rather constant QD spin lifetime, which could be governed by the spin dephasing time T_2^* . The observed rising in QD spin polarization degree could be likely attributed to a combined effect of shortening of trion lifetime and increasing spin injection efficiency from the WL. The latter may be caused by thermal activation of non-radiative carrier relaxation channels.

Populärvetenskaplig sammanfattning

I denna avhandling presenteras optiska studier av fenomen som rör spinnrelaterade mekanismer i kvantprickar. De kvantprickar som studerades är små kristaller av halvledarmaterial med en storlek av bara några tiotals nanometer (en miljondel av en millimeter). Dessa är ofta inbäddade i en större halvledarkristall av ett annat material. Den begränsade storleken av kvantprickarna har till följd att laddningsbärare som kan fångas in, så som elektroner och hål, kan bara inta vissa diskreta energinivåer. Denna situation liknar tillstånden i en atom, varför kvantprickar också kallas för artificiella atomer.

Elektroner som har fångats in i en kvantprick är så pass väl avskärmade från omgivningen att deras intrinsiska vridmoment, spinnet, bevaras under en lång tid. Tiden är tillräcklig lång att forskarna kan tänka sig använda spinnet inuti kvantprickarna till att spara och bearbeta information - kvantinformatiön - och bygga elektroniska kretsar som använder sig av spinnet som informationsbärare istället för enbart laddningen, som i dagens mikroelektronik. Denna forskningsgren kallas därför för spinntronik.

Spinntronik kan låta futuristiskt, men faktum är att spinntroniska komponenter finns redan nu i nästan alla datorers hårddiskar: det läshuvudet i hårddiskar använder sig av jättemagnetoresistans-effekten (GMR) för att läsa av information som sparats i magnetiska bitar på hårddisken. En annan spinntronisk komponent som redan tillverkas industriellt är magnetiskt random access memory (MRAM). Nästa stora språng i spinntronikens utveckling förväntas vara kvantkommunikation och kvantdatorer som överför och bearbetar information med hjälp av kvanttillstånd, så som fotonernas och elektronernas spinn. En pusselbit i detta långsiktigt arbete är att karakterisera spinnrelaterade mekanismer i halvledarkvantstrukturer, såsom kvantprickar och deras omgivande strukturer. I denna avhandling har några av dessa studerats med hjälp av optiska metoder som ger enkel och direkt tillgång till laddningsbärarnas spinninformation.

Förmågan att initialisera elektronernas spinn effektivt genom absorption av cirkulär polariserad ljus i kvantpricks-baserade halvledarstrukturer har studerats. Det har visat sig att excitoner har sämre förmåga att tillföra spinn från omgivande strukturer till kvantprickarna. Excitoner är kvasipartiklar bestående av en elektron och ett hål som är korrelerade genom en speciell kvantmekanisk växelverkan. Den så kallade utbytesväxelverkan möjliggör utbyte av rörelsemängdsmoment mellan elektron och hål, vilket leder till spinnrelaxation. Fria, okorrelerade elektroner och hål behåller

sin spinnorientering betydligt bättre och är därmed mera lämpade för att överföra kvantinformation i halvledarstrukturer. Vid excitering av vissa excitoniska tillstånd uppstår så kallade Fano resonanser där till och med en total förlust av förmågan att skapa spinnorienterade laddningsbärare i kvantstrukturer förekommer. Denna effekt kan kanske användas som en spinn modulator eftersom den förutses vara enkelt modulerbar genom ett elektriskt fält.

Ett externt magnetiskt fält kan betydligt förbättra kvantprickarnas förmåga att detektera laddningsbärarens spinnorientering, upp till en faktor av 2.5 i de strukturer som undersökts i avhandlingen. Denna förbättring beror på försvagning av de mekanismer genom vilka spinn relaxerar i kvantpricken. I speciella strukturer, bestående av två kvantprickar precis intill varandra, har det visat sig att odlingsmetoden också påverkar strukturernas spinnegenskaper. Strukturer av flera kvantprickar är intressanta för att undersöka kopplingen mellan flera kvantinformationsenheter (dvs spinn av laddningsbärare i de olika kvantprickar). En odlingsmetod för framställning av sådana strukturer med parallel orientering är baserad på självorganisation och utnyttjar mekaniskt stress för att styra tillväxtplatsen av kvantprickarna. Denna stress har visat sig öka spinnrelaxationen av laddningsbärarna innan de fångas in i kvantprickarna, vilket försämrar spinninjektionsförmågan i dessa strukturer.

De flesta undersökningar genomfördes vid låg temperatur, ofta bara några grader över den absoluta nollpunkten, för att minimera inflytandet av termiska kristallsvängningar på elektronernas spinn. Överlag så sjunker spinn polarisationsgraden i kvantprickarna på grund av dessa inverknings inom ett visst temperaturområde. Men, vid ännu högre temperaturer, som kan sträcka sig upp till rumstemperatur i vissa strukturer, har det visat sig överraskande, att spinn polarisationsgraden i kvantprickarna ökar skarpt. Möjliga mekanismer bakom detta beteende diskuteras.

Preface

The work presented in this thesis has been conducted during the time between November 2007 and February 2012 in the Functional Electronic Materials division at the Department of Physics, Chemistry and Biology at Linköping university, Sweden. The main motivation has been an in-depth characterization of spin-related processes in quantum dot based semiconductor nanostructures by optical and magneto-optical means.

The thesis is divided into two parts. At first, a general introduction into relevant areas of the scientific field is given, together with a description of applied characterization techniques and a summary of the obtained scientific results. The second part consists of the publications which present the main results in detail.

Publications included in this thesis

- 1 J. Beyer, I. A. Buyanova, S. Suraprapapich, C. W. Tu, W. M. Chen. Spin injection in lateral InAs quantum dot structures by optical orientation spectroscopy. *Nanotechnology* **20** (2009) 375401.
- 2 J. Beyer, I. A. Buyanova, S. Suraprapapich, C. W. Tu, W. M. Chen. Efficiency of spin injection in novel InAs quantum dot structures: exciton vs. free carrier injection. *Journal of Physics: Conference Series* **245** (2010) 012044.
- 3 J. Beyer, I. A. Buyanova, Bo E. Sernelius, S. Suraprapapich, C. W. Tu, W. M. Chen. Strong suppression of spin generation at a Fano resonance in a semiconductor nanostructure (2012). *Manuscript*.
- 4 J. Beyer, P.-H. Wang, I. A. Buyanova, S. Suraprapapich, C. W. Tu, W. M. Chen. Effects of a longitudinal magnetic field on spin injection and detection in InAs/GaAs quantum dot structures (2011). *Submitted manuscript*.
- 5 J. Beyer, Y. Puttisong, I. A. Buyanova, S. Suraprapapich, C. W. Tu, W. M. Chen. Temperature dependence of dynamic nuclear polarization and its effect on electron spin relaxation and dephasing in InAs/GaAs quantum dots (2012). *Submitted manuscript*.
- 6 J. Beyer, I. A. Buyanova, S. Suraprapapich, C. W. Tu, W. M. Chen. Strong room-temperature optical and spin polarization in InAs/GaAs quantum dot structures. *Applied Physics Letters* **98** (2011) 203110.
- 7 J. Beyer, I. A. Buyanova, S. Suraprapapich, C. W. Tu, W. M. Chen. Hanle effect and electron spin polarization in InAs/GaAs quantum dots up to room temperatures (2011). *Submitted manuscript*.

My contribution to the papers

For papers 1, 2, 3, 6 and 7, I performed all optical measurements and data analysis. For papers 4 and 5, I performed most of the optical measurements while some were conducted either in collaboration with or by the second author. I wrote all first manuscript versions.

Not included publications

- 1 J. Beyer, I. A. Buyanova, S. Suraprapapich, C. W. Tu, and W. M. Chen. Free-carriers beat excitons in spin-injection contest. Nanotechweb.org, 2009. Invited scientific summary at <http://nanotechweb.org/cws/article/lab/40357>.
- 2 J. Beyer, I. A. Buyanova, S. Suraprapapich, C. W. Tu, and W. M. Chen. Efficiency of spin injection in novel InAs quantum dot structures. In *Abstract Book of the 14th International Conference on Modulated Semiconductor structures (MSS-14)*, Kobe, Japan, July 2009.
- 3 J. Beyer, I. A. Buyanova, S. Suraprapapich, C. W. Tu, and W. M. Chen. Optical spin injection and spin detection in novel InAs quantum dot structures. In *Abstract book of the SPIE Microtechnologies conference, Prague, Czech Republic*, page 8068B–51, April 2011.

Acknowledgements

I would like to express my thanks to Prof. Weimin Chen and Prof. Irina Buyanova for giving me the opportunity to work in their group. I want to thank you for all invaluable, stimulating discussions and for always finding some light in the darkest maze of data.

I am grateful to Arne Eklund and Roger Carmesten for taking so well care of a continuous supply of liquid Helium and helping out with a multitude of other technical challenges of varying size.

Lejla Kronbäck, Eva Wibom and Anna Karin Stål were always helpful in all administrative issues - thank you very much for that.

I want to thank Dr. Daniel Dagnelund for sharing the office, countless discussions and chats on physical as well as other topics and for joint out-of-office activities. It was really great to have you around. Many thanks also to Yuttapoom Puttisong for all those *spinning* discussions. It is a pleasure to thank also all my other colleagues through the years, Dr. Deyong Wang, Shula Chen, Prof. Xingjun Wang, Dr. Qijun Ren, Dr. Sun-Kyun Lee, Stanislav Filippov and Po-Hsiang Wang for the great company.

I owe great thanks to Dr. Vladimir Kalevich for valuable help with my first Hanle measurements, and to Prof. Bo E. Sernelius for helpful discussions and his calculations concerning Fano resonances.

And thank you to all the other PhDs and PhD students for enjoyable joint coffee breaks and lunches.

Though at some distance, my parents and all the family always felt close, caring and supporting. I am truly thankful for that.

Thank you, my two daughters Samira and Camilla, for bringing so much joy and happiness into my life and for your unconditional love.

And thank you, Franziska - for your never-ending support and encouragement, for your true love and care through all the ups and downs. Thanks for your understanding whenever I was working late and for your strength in taking care of our family during our times of *dual residence*. I love you.

Jan

1	Semiconductor Physics	1
1.1	Crystalline structure of solids	1
1.2	Electronic structure of atoms	1
1.3	Band structure of bulk semiconductors	3
1.4	Band structure diagram	5
1.5	Heterostructures	8
1.5.1	Band alignment	8
1.5.2	Quantum confinement effects	8
1.5.3	Strain effects	10
1.5.4	QD growth	11
1.6	Single and multiple QD structures	12
1.7	Fano resonances	13
2	Spin Physics in QD Structures	15
2.1	Spin-orbit interaction	15
2.2	Spin structure of excitons and trions	16
2.3	Spin depolarization mechanisms	17
2.3.1	Electron-hole exchange interaction	20
2.3.2	Hyperfine interaction	20
2.4	Dynamic nuclear polarization	23
2.5	Effects of external magnetic fields	24
2.5.1	Landau levels	24
2.5.2	Zeeman splitting	25
2.5.3	Spin polarization in a longitudinal magnetic field	26
2.5.4	Spin depolarization in a transverse magnetic field	29
2.6	Effects of elevated temperatures	31
3	Methods	33
3.1	Light	33
3.2	Photoluminescence	34
3.3	Polarization optics	36
3.4	Photoluminescence of semiconductors	38
3.5	Photoluminescence excitation spectroscopy	39
3.6	Optical Orientation	40
4	Summary of Papers	43
	References	45

1 Semiconductor Physics

In this introductory chapter, an overview over many of the interesting and unique properties of semiconductors is given, mainly with the aim to describe their charge carrier band structure.

1.1 Crystalline structure of solids

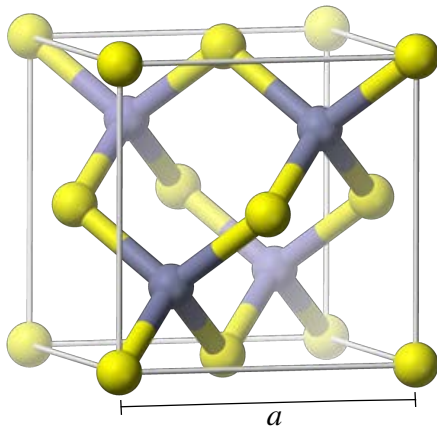
Crystals are solids that have a regular ordering of the constituent atoms with a certain symmetry in the atomic arrangement. In this thesis, only crystals in the traditional sense, possessing three-dimensionally periodic atomic arrangement and long-range order will be discussed. Quasicrystals, lacking long-range periodicity, will not be included. The smallest unit from which periodic crystals can be built up by repeating it in all three dimensions, is called the unit cell. It is spanned by three lattice vectors, whose lengths give the lattice constants in the respective directions.

A typical binary compound semiconductor crystal, i.e. one consisting of two species of atoms, is gallium arsenide (GaAs). It consists of Gallium (Ga) and Arsenic (As) atoms, all of which have four covalent bonds to four neighbouring atoms of the other species. These are distributed equally in space, pointing to the corners of a tetrahedron with the respective atom in its center.

Extending this structure three-dimensionally leads to the zincblende lattice structure, which is a cubic structure. Cubic denotes the fact that the three lattice vectors have the same length and are orthogonal to each other. The unit cell does not consist of a single tetrahedron, but four of them. Figure 1.1 shows a sketch of the unit cell of the zincblende structure.

1.2 Electronic structure of atoms

Atoms consist of a tiny nucleus, made up of protons and neutrons, and a number of electrons orbiting the nucleus at comparatively large distance. These electrons are, however, not free to orbit the nucleus at an arbitrary distance in any arbitrary way. They are found to occupy discrete shells associated with distinct (potential and kinetic) energy levels. Energies in between these allowed levels are not available for occupation by an electron in the respective atom. Yet, each shell may hold several electrons, if these occupy distinct electronic sublevels.



	GaAs	InAs
lattice constant a	0.565 nm	0.606 nm

Figure 1.1: **Left:** Sketch of the unit cell of a zincblende-type crystal (after [1]). The grey (dark) and yellow (bright) balls represent the two atomic species, e.g. Ga and As for GaAs. The lines between the balls are the covalent bonds. **Right:** The room temperature lattice constants for GaAs and InAs.[2]

All allowed (sub)levels are characterized completely by a set of quantum numbers, which is required to be unique for each of the atom's electrons. This postulate is known as the Pauli exclusion principle - no two electrons of a closed system are allowed to have an identical set of quantum numbers. For electrons in a free atom there are four quantum numbers:

- The **principal quantum number n** enumerates different electron shells of the atom. It ranges from 1 to infinity. The average distance of the electron to the nucleus increases with n .
- The **angular momentum quantum number l** enumerates different subshells within each shell. For the n th shell, n different subshells are found. These are labelled either by the value of l , ranging from 0 to $n - 1$ or by Latin characters of the following sequence: s, p, d, f, g... These subshells can be visualized by different shapes of the electron orbit. The s subshell is radially symmetric (sphere-like), the p subshells have a dumbbell-shape whereas the d and higher subshells have more complicated shapes.

- The **magnetic quantum number** m_l enumerates the specific orbital occupied within each subshell. It ranges from $-l$ through zero to $+l$ for the l th subshell. This may be represented by e.g. different orientations of the p subshell (where $l = 1$) dumbbells in the three perpendicular directions of the space (corresponding to $m_l \in \{-1, 0, 1\}$).
- In each uniquely characterized atomic orbital, with a unique set of the above three quantum numbers, two electrons are found to reside. These differ in their behaviour in magnetic field, which is characterized by a fourth quantum number. The **spin quantum number** s , which can only take two values, $+1/2$ or $-1/2$. Each electron can be imagined as possessing some kind of intrinsic magnetic moment (the spin), either pointing along a certain predefined direction or against it. In the following of this thesis, these two spin orientations will conventionally be referred to with the help of thin vertical arrows, \uparrow for $s = +1/2$ and \downarrow for $s = -1/2$.

In equilibrium, the electrons settle to the energetically lowest available state under consideration of the Pauli exclusion principle. Thus, after a long time and at very low temperature, there will be an abrupt boundary between the low-energy, fully occupied levels and the high-energy, empty levels.

Upon exchange of energy with its environment, the atom's electrons may change from one shell to another. For absorption of energy, an electron from an occupied shell will be excited into an empty level of a higher lying shell. For emission of energy, an empty level in a lower lying shell is needed, so that an electron from an occupied level of a higher lying shell can relax there. These transitions typically take place by exchanging energy via an electromagnetic field - i.e. light. The corresponding quasiparticle is called a photon. As a photon carries not only energy, but also angular momentum (which will be discussed further in section 3.1), the (angular) momentum conservation law results in further restrictions on the allowed transitions. These restrictions are called selection rules.

1.3 Band structure of bulk semiconductors

If atoms are brought sufficiently close to each other, their electrons will start to interact. This interaction affects the energies of the s- and p-levels of the outermost shells

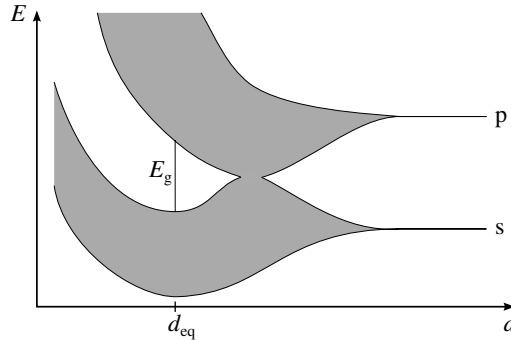


Figure 1.2: Evolution of energy bands from the outermost atomic s- and p-levels as a function of interatomic distance d . The equilibrium distance d_{eq} and the corresponding energy band gap E_g are indicated.

in such a way, that the confined atomic energy levels merge into extended electron levels. Their energies rearrange over a small range in energy, forming an energy band. Energy bands originating from different atomic levels may still be separated by energy intervals, where no electronic levels are available. These energy gaps are called the band gaps, denoted by E_g .

In figure 1.2, this evolution of the energy levels in the outermost s- and p-subshells of a particular type of atoms into energy bands is depicted. When many atoms are arranged in a periodic lattice with an interatomic distance d , where d is very large initially, then no interaction is present and corresponding electron levels in the different atoms will all have exactly the same energy. This situation is shown at the right side of the diagram. Reducing d , the interaction between the electrons increases and their energy levels spread out over the energy bands. Bringing the atoms even closer, these bands may cross and even split again. At some certain distance, the energy of the lower band reaches a minimum, before it starts to rise again due to strong Coulomb repulsion. The position of this minimum in energy depends on the specific type of atoms involved and it will be the equilibrium interatomic distance d_{eq} of the respective material.

All atoms taking part in the interaction form a new closed system, for which the Pauli exclusion principle is valid again. So the available electrons will fill up all lower energy levels. In an intrinsic semiconductor at zero temperature, the highest occupied band is called the valence band (VB) and it will be fully occupied by electrons. The VB is separated by the band gap energy E_g from the completely empty conduc-

tion band (CB). Electric conductivity is not possible, because the electrons do not have enough energy to be excited into the empty levels of the CB.

At a finite temperature, thermal activation of some electrons from the VB into the CB will enable electrical conductivity, so that these materials are no longer completely isolating. Furthermore, the amount of electrons in the CB can be controlled by adding certain atoms having filled electronic levels that can donate electrons into the CB of the host material. Such atoms, and their corresponding electronic levels, are referred to as donors. Other atoms, called acceptors, may in turn be able to accept electrons from the VB easily, thus creating empty levels in the VB, called holes. This will enable electrical conductivity in the VB. The addition of either donors or acceptors is called doping and the respective atoms are the dopants. Doping provides a variation of the total conductivity of a semiconductor in a very wide range, which is the basis of the overwhelming success of these materials in today's electronic industry.

1.4 Band structure diagram

The spatial periodicity of the atoms in a crystal has profound consequences for its electronic properties. Due to the interaction between the atoms, the electrons are actually no longer localized to a single orbit around a single nucleus. The probability to find the electron at a certain position \vec{r} in space is given by a probability function $|\Psi(\vec{r})|^2$. $\Psi(\vec{r})$ is called the wave function of the particular electronic state.

$\Psi(\vec{r})$ takes a special form in periodic crystals, called a Bloch function. The Bloch theorem states, that the wave functions in a periodic potential are a product of two components:

$$\Psi_{\vec{k}}(\vec{r}) = u_{\vec{k}}(\vec{r}) \exp(i\vec{k} \cdot \vec{r}) \quad (1.1)$$

The first component $u_{\vec{k}}(\vec{r})$ has the periodicity of the underlying crystalline lattice whereas $\exp(i\vec{k} \cdot \vec{r})$ is a plane wave, which would be the wave function for a free electron.

The index \vec{k} enumerates the wave functions possessing different wave vectors \vec{k} and thus different crystal momenta $\vec{p} = \hbar\vec{k}$.

When electrons in a periodic lattice are accelerated, e.g. in an external electric field, then the crystal momentum $p = \hbar k$ changes and accordingly also their kinetic energy

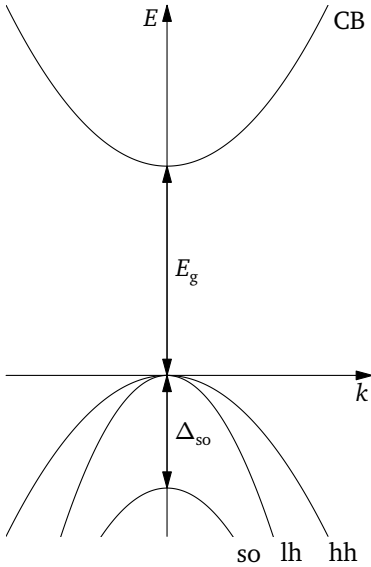
$$E = \frac{p^2}{2m} = \frac{\hbar^2 k^2}{2m} \quad (1.2)$$

The relation $E(k)$ is called dispersion relation. For electrons near the bottom of the CB of typical semiconductors, it is often rather well described by a parabola, as given above. However, the effect of the periodic lattice of atoms changes the apparent mass of the electron. So m in the above equation is not the value of the free electron's rest mass, but typically only a fraction of it. Conventionally, the value of this effective mass m^* is given in units of the free electron mass m_0 . m^* may actually depend both on direction and speed of the electron motion in a crystal, resulting in non-parabolic and anisotropic $E(k)$ dependencies. This is most pronounced for carriers in the VB, where the dispersion relation often turns out to follow a parabolic law only for rather small k . The non-parabolicity at higher k and the dependence on the direction of electron motion can be described by the effective mass itself being a function of the electron wave vector \vec{k} .

In contrast to the CB, the VB also consists of several subbands, originating from the degeneracy of the atomic p-states of the host lattice (where originally $l = 1$ and $m_l \in \{-1, 0, 1\}$). The spin-orbit interaction, to be discussed in section 2.1, couples the spin and angular momentum in these bands and splits off one of them by the spin-orbit interaction energy Δ_{so} , the spin-orbit split-off band, typically denoted by so. The other two are still degenerate for $k = 0$ but split for $k \neq 0$, each following, to a first approximation close to $k \approx 0$, a parabola, but with different coefficients $\hbar^2/2m^*$. According to these, the two subbands are labelled the heavy-hole and the light-hole bands, typically denoted by hh and lh, respectively. The hh band shows a weaker bending, corresponding to a larger effective mass m_{hh}^* , whereas the lh band shows a stronger bending with a lower effective mass m_{lh}^* . A sketch of typical dispersion curves, which make up the band structure diagram, is shown in figure 1.3.

The VB maximum is usually located at $k = 0$. This is not necessarily the case for the CB minimum. If the latter is also located at $k = 0$, the semiconductor is called a direct band gap semiconductor. Examples are GaAs and InAs. Carrier transitions between the CB minimum and the VB maximum are possible without a change in k . But many semiconductors exhibit a CB minimum which is not located at $k = 0$. These are called indirect band gap semiconductors. Prominent examples are silicon and germanium. Carrier transitions between the CB minimum and the VB maximum require here a change in the carrier's momentum k . This can be provided by phonons. For

1.4 BAND STRUCTURE DIAGRAM



	GaAs	InAs
band gap energy E_g	1.519 eV	0.417 eV

Figure 1.3: Left: Band structure diagram for a typical direct band gap semiconductor. Right: Low temperature band gap energies for GaAs and InAs. [2]

optical applications, this requirement of phonon assistance is disadvantageous, as it reduces the radiative recombination efficiency. Thus direct band gap semiconductors are preferred in this case.

As discussed above, the VB is completely filled by electrons at zero temperature whereas the CB is empty. Absorption of energy larger than the band gap energy E_g leads to excitation of an electron from the VB to the CB. In external fields, the free electron responds according to the CB dispersion relation, whereas the empty state in the VB represents the collective response of all remaining electrons there. It turns out, that this behaviour can be adequately described by considering the empty state as a particle of positive charge $+e$, with e being the elementary charge. This quasiparticle is called a hole and lends its name to the different VB subbands. Upon relaxation of the free electron back into the empty state of the VB, the hole disappears. This process has been termed recombination of electron and hole.

1.5 Heterostructures

1.5.1 Band alignment

The above discussion of the electronic band structure concerned a homogeneous bulk semiconductor material. A heterostructure is created by growing two different semiconductors on top of each other, assuming that this is possible without too many structural defects occurring due to either different crystal structures or different lattice constants. In such structures, the relative energetic positions of the CB and VB edges will determine in which material the respective free carriers will have their lowest energy state. Generally, both band edges will exhibit a discontinuity at the interface of the two materials.

Growing e.g. InAs, with a band gap energy of 0.415 eV (at low temperature), on top of GaAs, which has a band gap of 1.519 eV, both CB and VB will share the total band offset. In such a configuration, called Type I band alignment, both electrons in the CB and holes in the VB will have their lowest energy state in the material with the lower E_g , i.e. InAs. A sketch of such a band alignment is shown in the left panel of figure 1.4. Type I band alignment is advantageous for optical processes, as under optical excitation of the near-interface region both types of carriers will be confined in the same (the InAs) layer, providing high recombination probability due to the stronger wave function overlap of electrons and holes.

Of course, also other band alignments are possible. In Type II band alignments, both the CB and the VB edge are offset in the same direction, leading to a separation of electrons and holes across the heterostructure interface. In Type III, finally, the two band gaps do not overlap at all.

1.5.2 Quantum confinement effects

Extending a heterostructure to three layers, e.g. by sandwiching a sufficiently thin InAs layer between two GaAs layers, carrier wave functions in the InAs may be compressed by the presence of the large potential energy barrier to the GaAs. The InAs layer is then called a quantum well (QW). Such quantum confinement of carriers results in a quantization of their energy levels accompanied by a shift towards increasing energies. The energy shift is called confinement energy and effectively increases the observed band gap energy. Thus the lowest electron and hole states in an InAs

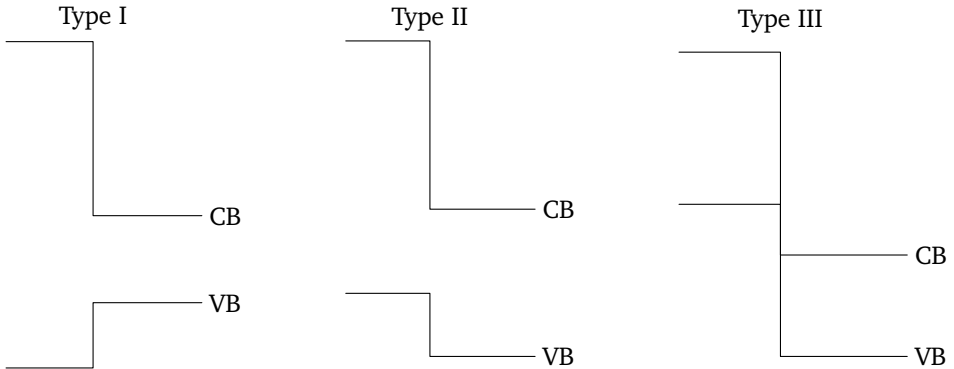


Figure 1.4: Sketch of the three types of band alignments at heterostructure interfaces. Shown are the band edge energy positions on the vertical axis, over a spatial direction across the heterostructure interface on the horizontal axis .

quantum well will not have an energetic difference corresponding to the bulk InAs band gap of around 0.4 eV, but actually much higher, with the exact value depending on the strength of the quantum confinement, i.e. the thickness of the InAs layer. As the carriers in a QW are only confined in the direction perpendicular to the QW plane, their in-plane motion is still free, and follows a two-dimensional dispersion. This creates an energy continuum of states above each of the quantized levels.

Quantum dots (QDs), on the other hand, are nanosize crystals of a material where the carriers are strongly confined in all three dimensions. This leads to a suppression of the continua and atomic-like, fully quantized, energy states. As often the confinement potential is approximately parabolic, these levels are approximately equidistant.

Besides the total shift of the electron and hole energy levels due to their respective confinement energies, also the degeneracy of the hh- and lh-VB at $k = 0$ will be split. This split is caused by different confinement energies for hh and lh due to their different effective masses.

When exciting an electron from the VB into the CB, both the free electron in the CB and the hole in the VB may relax to the thin InAs layer, as the InAs-GaAs-system shows a Type I band alignment. The spatial proximity of these two (quasi)particles of opposite charge leads to Coulomb attraction between them. This interaction creates a new, hydrogen-like, bound state of the electron-hole-pair, called exciton. Upon recombination, the emitted energy is slightly lower than the energy difference between

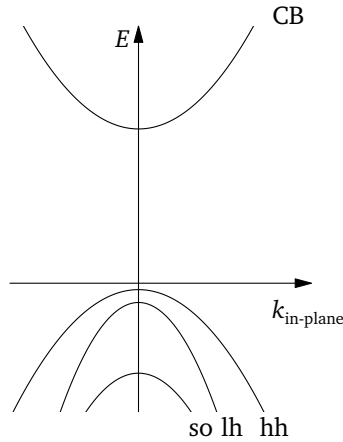


Figure 1.5: Band structure diagram for a direct band gap semiconductor under compressive strain, showing the splitting of the hh and lh VB at $k = 0$.

the non-interacting electron and hole levels, due to the positive exciton binding energy. This leads to the dominance of excitonic features in optical spectra at low temperatures.

1.5.3 Strain effects

Often, lattice constants between two different materials differ, so that at their heterostructure interface, the material with the smaller lattice constant will need to expand slightly and the other material will be compressed in the plane of the interface. The resulting strain has a profound influence on the electronic structure and the energy bands.

In the InAs/GaAs case, the InAs layer is compressively strained, as the InAs lattice constant is approximately 7% larger than the GaAs one. Following figure 1.2, the resulting compressive strain will increase the band gap energy and shift the energy levels in the InAs layer towards higher energies. Additionally, the hh and lh VBs which are degenerate at $k = 0$ in bulk, split apart so that the energy for holes in the lh VB is raised whereas the energy for hh is lowered. In the band structure diagram, this is represented by a relative upward shift of the hh VB and a relative downward shift of the lh VB, see figure 1.5.

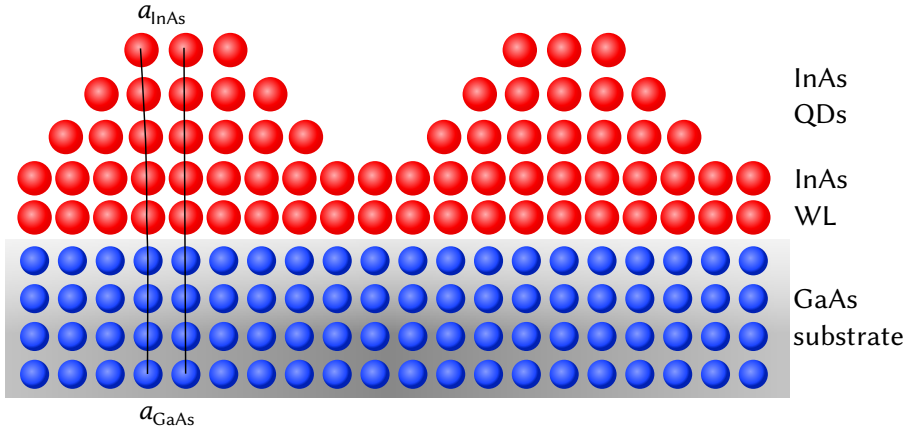


Figure 1.6: Sketch showing the relaxation of the compressive strain in the InAs layer through formation of small islands during Stranski-Krastanov-growth mode (based on [3]).

1.5.4 QD growth

Strain is actually also the driving force for the growth of self-assembled QD structures to be discussed in the following.

As mentioned above, growing InAs on top of a GaAs substrate, which is typically oriented along the [001] direction, results in a rather large compressive strain due to the lattice constant mismatch of around 7%. Such large strain cannot be accommodated coherently in a perfect crystal, and after a thickness of a few atomic layers of InAs, the strain will relax. This strain relaxation yields growth of InAs islands instead of layer-by-layer deposition. In the small InAs islands, the lateral lattice constant can relax towards the larger InAs value, as illustrated in figure 1.6. As a result, self-assembled InAs islands, the QDs, are grown residing on a thin InAs wetting layer (WL). Such a growth mode is called the Stranski-Krastanov (SK) growth mode. The WL is in fact a strained QW. Thus self-assembled SK InAs/GaAs QD structures contain the following three major components: the GaAs substrate and capping layer, the InAs WL and the InAs QDs.

It should be noted, that neither the WL nor the QDs are purely InAs. During growth and capping by a protective GaAs capping layer, Ga diffuses into the InAs layers, forming an InGaAs alloy. The Ga-concentration has even been found to show a gradient along the growth direction in the QDs. The main consequence of this intermixing is a further opening of the band gap of these structures, in addition

to the modifications due to strain and quantum confinement. The Ga gradient in the QDs has also been found to separate electron and hole states along the growth direction.[4; 5]

Typically a GaAs capping layer is grown on top of the InAs QDs for protection. For some of the sample structures studied in this work, the GaAs capping layer was kept very thin. The resulting strain, which is now also acting from the top onto the InAs QDs, transforms them into rings.[6] By continuing the deposition of further InAs on top of these rings, novel laterally arranged multiple QD structures can emerge. Depending on the InAs regrowth temperature, either all-aligned double QD structures or rings of five to seven QDs have been found.[6; 7] A set of these samples has been studied in this thesis work.

1.6 Single and multiple QD structures

The three-dimensional carrier confinement in QDs makes them a very interesting and currently actively researched target for a variety of studies. As no energy bands exist any longer, the notion of a \vec{k} -vector gets inappropriate and carriers behave similar to electrons in a single atom again. However, there is the benefit, that these artificial atoms are designable. The exact carrier confinement is tunable via e.g. the QD size, that can be controlled straightforwardly during growth. This enables controllable studies of atomic-like physics in a solid state environment.

Due to the strong carrier confinement, excitonic effects are well pronounced in QDs. The recombination probability is high due to the large wavefunction overlap between electron and hole, which makes QDs ideal for photonic applications. Lasers, e.g., benefit from these characteristics by a reduced lasing threshold.

As will be discussed later in chapter 2, the suppression of carrier motion and related scattering also leads to a high stability of the carrier's spin orientation. Therefore application of QDs in quantum information technology[8] and spintronics[9] has been proposed, where the spin degree of freedom is envisioned to replace or enhance the charge that is currently used to transmit and manipulate information in micro-electronics.

Multiple QD structures are interesting as they allow the study of interaction of separately confined carriers and excitons. Two tunnel-coupled QDs have been proposed as a source of entangled photons with the advantage of emitting the two pho-

tons from separated QDs[10]. Generally, multiple QD structures may be particularly suitable for studying spin interactions that constitute the basis for quantum computing applications.

1.7 Fano resonances

The appearance of discrete energetic levels resulting from either quantum confinement or excitonic transitions, together with absorption continua allows the study of an interesting phenomenon that was initially studied in atomic ionization spectra - the interference of two concurrent excitation/scattering pathways. Interference is well-known to occur whenever a scattered wave can propagate along two possible paths and combine again. Relative phase shifts in the two scattering channels can lead to resonant enhancement and suppression of the total transmission and result in a pattern of constructive and destructive interference. The special case of a Fano resonance emerges when the scattering can occur both via an energetically discrete transition and via an overlapping continuum of transitions. Then the wave nature of the scattered particle results in constructive and destructive interference of the two scattering paths in the spectral vicinity of the discrete scattering level.

In the original description of Fano[11] an atomic discrete state was considered with its energy lying above the first ionization energy of the atom. The corresponding absorption line shape had been found to be strongly asymmetric, which could be described by interference between two alternative mechanisms of excitation. The two mechanisms are the excitation of the discrete atomic level and the ionization continuum. Fano's derivation resulted in a formula describing the asymmetric absorption line shape:

$$I(\mathcal{E}) \propto \frac{(q + \mathcal{E})^2}{1 + \mathcal{E}^2} \quad (1.3)$$

The absorbed photon energy is given here as a scaled dimensionless energy $\mathcal{E}(E) = (E - E_d) / (\Gamma/2)$ with E_d being the actual energy position of the discrete level and Γ its spectral width. The Fano parameter q describes the strength of the asymmetry, which, from theory, is proportional to the ratio between the transition strength to a modified discrete state and the transition strength to the continuum.

Fano resonances have been found to be almost ubiquitous, generating extensive literature and a very recent comprehensive review[12] that particularly focussed

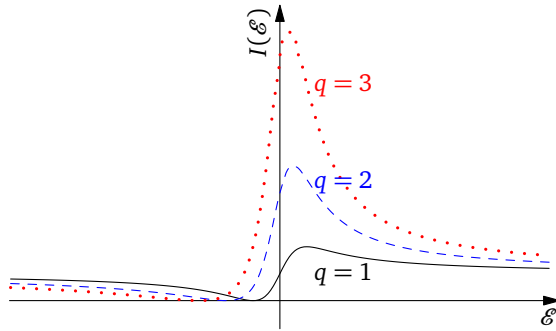


Figure 1.7: Line shapes of Fano resonances according to equation (1.3) for several Fano parameters q .

on nanostructures. In QW structures, Fano resonances were observed at positions, where a higher lying discrete excitonic transition overlaps with a continuum of states from a band-to-band-transition of a lower band.[13; 14] Also in electron transport spectra through continuous quantum channels, containing an embedded QD, Fano resonances have been identified theoretically[15] and verified experimentally[16].

The necessary interaction between the discrete state and the continuum, which leads to the appearance of the Fano resonance, has typically been treated as spin-conserving, thus coupling only states of the same spin orientation. Theoretical proposals for spin filtering with Fano resonances[17–19] required an external field to split the two spin states of the discrete level, leading to a spin-split Fano resonance. Transmission of one spin orientation would then be suppressed at the dip of its corresponding Fano resonance. Both external magnetic and effective fields originating from spin-orbit coupling have been considered for the spin splitting.

But also the direct interaction between a continuum and a discrete state of opposite spin orientations can lead to Fano resonances, which has been considered theoretically, e.g. in [20; 21]. It has been furthermore shown, that a local spin-orbit coupling scattering potential alone is able to generate a Fano resonance, by separating a discrete state of one spin orientation and coupling it to the continuum of opposite spin orientation.[22]

2 Spin Physics in QD Structures

In the previous chapter, a general introduction to the electronic level structure of semiconductors and especially of semiconductor quantum structures has been given. To describe it, the first three quantum numbers, namely the principal quantum number, the angular momentum quantum number and the magnetic quantum number, have been (mostly) sufficient. In the current chapter, the description will be extended by considering the consequences of interactions with the fourth quantum number, the spin.

2.1 Spin-orbit interaction

Classically, any moving particle, e.g. an electron, in an external electric field, e.g. that of its nucleus, will experience also a magnetic field. This is, because in the electron's rest frame the nucleus is seen to circle around it. A moving charge creates a current, which is always accompanied by a surrounding magnetic field.

This effective magnetic field interacts with the electron's spin magnetic moment. As the effective magnetic field is parallel to the orbital angular momentum \vec{L} , it changes with the particular orbit that the electron is in. Thus the interaction with the spin angular momentum \vec{S} will be different for each electron state, where the interaction energy can be written as $\propto \vec{L} \cdot \vec{S}$. The proportionality constant is dependent on the particular electron state. In solids, this spin-orbit interaction depends correspondingly on the carrier's k -vector and its band.

This interaction energy couples the previously separate terms for \vec{L} and \vec{S} in the Hamiltonian, resulting in that these two are no longer conserved separately, but only the total angular momentum $\vec{J} = \vec{L} + \vec{S}$. For the corresponding quantum number j of the eigenstates, which gives the total angular momentum in units of \hbar , it follows $|l - s| \leq j \leq l + s$. Thus the CB, where $l = 0$, is still doubly degenerate as $j = s = 1/2$. In the VB, however, $l = 1$ and consequently $j \in \{1/2, 3/2\}$. The VB splits into a doubly degenerate spin-orbit split-off band, with $j = 1/2$, and the heavy and light hole bands with $j = 3/2$ where the corresponding projection of the total angular momentum on a preferential axis $j_z \in \{-3/2, -1/2, 1/2, 3/2\}$.

This coupling of spin and orbital angular momenta and its resulting energy splitting is, what finally enables optical orientation of carrier spins in semiconductors, to be discussed in section 3.6, as the photon does not couple to the carrier spins directly. On the other hand, as pure spin states are generally no longer the eigen-

states of the Hamiltonian, the spin-orbit coupling is also responsible for many spin relaxation mechanisms.

2.2 Spin structure of excitons and trions

In semiconductor quantum structures, both strain and quantum confinement split the remaining degeneracy of the hh and lh VBs as presented in section 1.5.3. Thus in the InAs/GaAs system, the hole ground state has hh character, i.e. $j_z = \pm 3/2$. This allows two hole states, which are typically denoted by double arrows: $\uparrow\uparrow$ where $j_z = +3/2$, originating from $m_l = +1$ and $s = +1/2$, and $\downarrow\downarrow$ where $j_z = -3/2$, originating from $m_l = -1$ and $s = -1/2$. Together with the two spin states of an electron in the CB, four combinations are possible for a neutral free hh exciton X^0 : $\uparrow\uparrow$, $\downarrow\uparrow$, $\uparrow\downarrow$ and $\downarrow\downarrow$. The total angular momentum J of these four combinations is (again given in units of \hbar) $J_{\text{tot}} = j_z^{e^-} + j_z^{\text{hh}} = +2, +1, -1, -2$, respectively. For brevity, these states are conventionally denoted by their total angular momentum value in a ket: $|\pm 2\rangle$ and $|\pm 1\rangle$. The $|\pm 1\rangle$ excitonic states are called bright states, as they can be excited directly from the crystal ground state (no exciton) by absorption of one photon (with angular momentum $\pm 1\hbar$). They can also decay radiatively by emission of a photon. The $|\pm 2\rangle$ states are optically inactive due to their larger angular momentum, thus they are called dark states.

It follows, that quantum wells, such as the InAs WL, due to their hh-lh VB splitting are well suited for excitation of spin oriented excitons and carrier pairs. The angular momentum of a circularly polarized photon, e.g. $+1$, can excite electrons from the hh VB to the CB, creating only $|+1\rangle$ electron hole pairs, corresponding to $\downarrow\uparrow$ spin states of the electron and hole. This enables efficient optical generation of spin oriented carriers and constitutes the basis of optical orientation measurements.

The given excitonic states are eigenstates only for systems of rather high symmetry. In QDs, often the real crystal and geometric confinement symmetry is reduced so that these excitonic states are no longer eigenstates. The anisotropic part of the electron-hole exchange interaction then results in different eigenstates, which can be described by a superposition of both states. Exchange interaction will be discussed in section 2.3.1 in more detail, but its result is that typically the optically active ground state of a neutral QD exciton is linearly polarized. Only in strong magnetic fields

the higher symmetry is effectively restored by the magnetic confinement. Then the ground states will be circularly polarized $|\pm 1\rangle$ again.

Due to either residual or intentional dopant carriers that will collect in the QD ground state, the QD ground state may already be populated by a hole or an electron before generation or capture of an optically excited electron-hole pair. The resulting entity is called a trion - a state consisting of either two electrons and a hole (X^-) or two holes and an electron (X^+). In a trion, the electron-hole exchange interactions cancel, as the single carrier always interacts with two other carriers of opposite spin orientation. Here anisotropy does not couple the two spin states. This property makes trions attractive for spintronic applications. Particularly, positive trions X^+ have been suggested and applied as efficient spin detectors.[23].

2.3 Spin depolarization mechanisms

After having created an initial population of spin polarized carriers, e.g. by optical orientation as described above, these carriers will relax both their energy and momentum and finally reach the ground state of the system, which is the QD ground state in our case. Both during this carrier relaxation, but also during the finite lifetime in the QD ground state the spin orientation will be affected by interactions with the environment. Typically these interactions will lead to a reduction of the spin polarization degree - spin relaxation occurs. But there are also scattering processes that prevent spin orientation loss.

Loss of spin orientation, also called spin depolarization, may be caused by two classes of processes: spin relaxation and spin dephasing. As the spin can be seen as a kind of magnetic moment, its interactions can be understood as results of interactions with external magnetic fields. These do not necessarily need to be real magnetic fields, but may also be effective magnetic fields, that provide a description of the effects of spin-orbit, exchange or hyperfine interactions.

Spin relaxation in its more narrow sense, denotes the transition of a spin orientation towards its equilibrium orientation under exchange of both energy and angular momentum with its environment. For an initially oriented ensemble of spins, generated e.g. by optical orientation, at zero external magnetic field, the equilibrium condition would be an equal number of up- and down-spins, i.e. the absence of ensemble spin polarization. The time required to reach this state is typically denoted

by T_1 , called the (longitudinal) spin relaxation time. In the presence of an external magnetic field, the two spin states will experience a Zeeman splitting, and the equilibrium population of both states will be determined by the Boltzmann distribution, leading to a non-zero equilibrium spin polarization.

Spin dephasing, on the other hand, is connected to the precession of spins in an external (effective) magnetic field that is at a certain angle to the spin orientation. The spin precession around the field conserves its projection onto the field direction. But the spin component perpendicular to the field, called transverse component, rotates around the field vector, its orientation at a particular moment in time being given by a certain phase angle. In an ensemble of spins in a semiconductor, such (effective) magnetic fields may be oriented randomly and may also change with time. The field variations in time will lead to random variations of the spin precession frequency for each single spin, which will randomize its phase angle, and thus the transverse spin component, with a dephasing time T_2 . Averaged over the spin ensemble, the transverse spin components may dephase faster due to spatially varying precession axes and frequencies. This is described by a characteristic transverse spin decay time T_2^* , the ensemble spin dephasing time. Such phase losses are reversible and may be eliminated by spin-echo experiments. In contrast, the randomization of the phase angle of each spin, described by T_2 , is irreversible. Typically $T_2^* < T_2$, so that the spin dynamics observed in e.g. QD ensembles are dominated by T_2^* .

It should be noted, that sometimes the term spin relaxation is also used in a wider meaning, encompassing all effects leading to a reduction of an initially prepared spin orientation. For clarity, the term spin relaxation in its more narrow sense may then be specified as longitudinal spin relaxation.

Three mechanisms are known for spin relaxation of free CB electrons in non-magnetic zincblende semiconductors,[24] such as studied in this thesis:

Elliott-Yafet mechanism: The electrical field which accompanies lattice vibrations or charged impurities interacts via spin-orbit interaction as an effective magnetic field, similar to the introductory discussion above for the nuclear electric field. Thus momentum relaxation (by phonons or impurity scattering) is accompanied by spin relaxation. The spin rotates only *during* the interaction/collision, as the effective field is zero otherwise. Spin relaxation by phonons is typically rather weak, especially at low temperatures. Spin relaxation by impurity scat-

tering depends on the scattering cross section/impact parameter and is proportional to the impurity concentration.

Bir-Aronov-Pikus mechanism: The scattering of CB electrons by an unpolarized population of holes can result in spin exchange via their exchange interaction, which leads to electron spin relaxation. This mechanism is relevant mainly in strongly p-type doped structures at low temperatures.

Dyakonov-Perel mechanism: In semiconductors lacking inversion symmetry (like GaAs and InAs), the CB is actually nondegenerate for $\vec{k} \neq 0$ in many crystalline directions. This spin splitting can be taken as the effect of a \vec{k} -dependent effective magnetic field arising from spin-orbit coupling. Thus electron spin precession will occur around different directions after every momentum scattering step, which will eventually lead to a randomization of the electron spin. In contrast to the Elliot-Yafet spin relaxation mechanism, the spin rotates now *between* collisions, thus its spin relaxation time will decrease with decreasing momentum scattering, e.g. decreasing impurity concentration.

The first two mechanisms usually make minor contributions. There the spin relaxation rate is proportional to the electron scattering rate. For the Dyakonov-Perel mechanism, the spin loss occurs between the scattering events, and thus the relaxation rate is inversely proportional to the scattering rate and usually dominates spin relaxation in bulk and 2D quantum structures.

In QDs, where the carrier motion is effectively suppressed, scattering events are rare and the carrier momentum \vec{k} is not well defined. Thus the efficiency of the above mentioned spin relaxation mechanisms is strongly reduced. This leads to very long spin relaxation times, that are mainly determined by two other mechanisms at low temperature:

exchange interaction: The Coulomb exchange interaction between the confined carriers in a QD leads to exchange of angular momentum between them, sometimes called spin flip-flops, effectively relaxing each carrier's spin.

hyperfine interaction: The hyperfine interaction of (mainly) the electrons in a QD with the nuclear spins leads both to longitudinal spin relaxation and spin dephasing.

2.3.1 Electron-hole exchange interaction

The exchange interaction (EI) consists of two parts, an analytical part (also called short-range part) and a non-analytical part (also called long-range part).[25] The long-range part can be thought of as arising from the electric field created by the excitation of the electron-hole pair, whereas the short-range part is of the form of a contact interaction between the electron and the hole spin.[26] Both parts contribute to a fine-structure splitting δ_0 between the bright $|\pm 1\rangle$ and dark $|\pm 2\rangle$ excitonic states. A further splitting δ_1 between the two bright excitonic states is caused by an anisotropic contribution to both short-range and long-range EI, abbreviated AEI.[27]

The anisotropy can originate from either geometrical shape anisotropy of the confining potential or from the low crystal symmetry at the atomic level. Actually two new eigenstates are created by AEI from the optically active states, being $|X\rangle = (|+1\rangle + |-1\rangle)/\sqrt{2}$ and $|Y\rangle = (|+1\rangle - |-1\rangle)/i\sqrt{2}$. [24] These are a superposition of the two original, circularly polarized, excitonic states, and they are linearly polarized, typically along the $[110]$ and $[\bar{1}\bar{1}0]$ directions. The splitting δ_1 of the neutral exciton X^0 in a QD has been observed in single-QD transmission spectroscopy, see Figure 2.1.[28] In the left panel, two transmission traces taken under orthogonal linear polarizations of the incoming light are shown in black and grey. Each polarization state is absorbed by only one of the two fine structure levels. Their relative energetic distance is given on the top ordinate and amounts to somewhat less than $20 \mu\text{eV}$. In the right panel, the absorption line of a negatively charged trion X^- is seen, which consists of two spin-paired electrons and a single hole in the X^- ground state. As EI is cancelled due to the electron spin pairing, no AEI splitting of this line is observed. Similarly, for a positively charged trion X^+ , no AEI splitting would be observable.

It is concluded, that only singly charged trions can carry spin information, whereas neutral excitons due to their AEI do not represent pure spin states.

2.3.2 Hyperfine interaction

An electron spin interacts with an ensemble of n nuclear spins via the hyperfine contact interaction $H_{\text{hf}} = \sum_n a_n (\vec{s} \cdot \vec{I}_n)$ where the constant $a_n \propto A_n |\Psi(\vec{r}_n)|^2$ with A_n being the hyperfine constant and $\Psi(\vec{r}_n)$ the envelope wave function of the electron at the position of the n th nucleus. For holes, this interaction is smaller, as the lattice-periodic part $u_{\vec{k}}(\vec{r})$ of their wavefunction has p-symmetry, thus showing a zero-crossing at

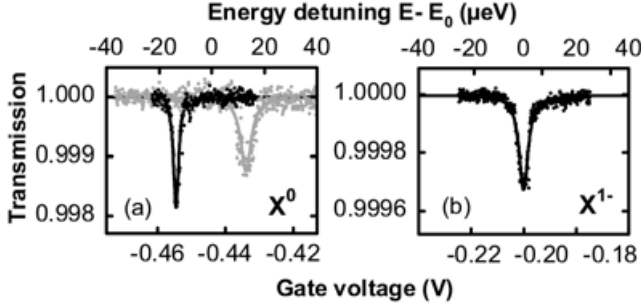


Figure 2.1: (a) Differential transmission spectra of the neutral exciton X^0 in a single self-assembled InGaAs/GaAs QD. The two curves have been taken under two orthogonal linear polarization states of the light and show the AEI splitting of the bright exciton ground state. (b) For the trion X^{1-} , no AEI splitting is observed.[28] Copyright 2004 by The American Physical Society.

each nucleus. Still, holes have been found to couple to the nuclear spins via the dipole-dipole hyperfine interaction, resulting in approximately one order of magnitude smaller hyperfine coupling as compared to electrons.[29]

Effects of the hyperfine interaction can be divided into dynamic and static ones.[30, Ch. 9] Dynamic effects allow transfer of angular momentum between the electron and the nuclear spin system, spin flip-flops, which under continuous pumping of electron spins leads to dynamic build-up of nuclear polarization. For an initially polarized electron spin system, this constitutes spin loss and is thus a spin relaxation mechanism. The effect on the nuclear spin system will be discussed in the following section 2.4. Static effects, on the other hand, are related to the response of electron and nuclear spins in the effective magnetic field of the other species[31] and will be summarized in the following.

For polarized nuclear spins, the electrons experience a quasistatic effective magnetic hyperfine field B_N , called the Overhauser field. It acts similar to an external magnetic field by causing a Zeeman splitting of the electron spin levels and precession of the electron spin. For a typical III-V QD, the Overhauser field of completely polarized nuclei may amount to up to a few Tesla of magnetic field strength.

Under usual conditions, nuclear spin polarization is extremely low, though, as the Zeeman splitting of the nuclear spin levels is around three orders of magnitude smaller than the electron's. This leads to very small population differences in ther-

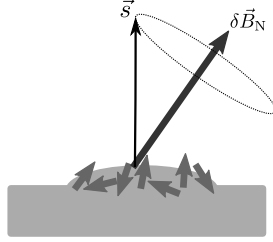


Figure 2.2: Illustration of electron spin \vec{s} precession in the frozen field of the hyperfine fluctuations $\delta\vec{B}_N$ at a certain instant of time. $\delta\vec{B}_N$ is constructed from the sum over all individual nuclear spin orientations in the QD, indicated by the short thick arrows, at that time.

mal equilibrium. Thus the nuclear spins are typically oriented randomly, causing only a small time-dependent net hyperfine fluctuation field $\delta\vec{B}_N$, which scales with the square-root of the number of nuclear spins within the electron wave function. Its typical strength is in the range of a few tens of milli-Tesla.[32] As $\delta\vec{B}_N$ changes only slowly with time, in comparison to typical radiative lifetimes in QDs, it can be considered as fixed for a given electron in a given QD. The term frozen nuclear spin fluctuations is often used to indicate that. An electron spin dephasing effect is caused by a varying $\delta\vec{B}_N$ over the QD ensemble and over longer times.

For randomly distributed nuclear spins in a QD ensemble, this will decrease the total electron spin polarization to one third of the initial value. This is because the fluctuation fields distribute over the three spatial dimensions, where one of them will be along the electron spin orientation and will not act spin depolarizing. The precession of the electron spins in the frozen fluctuations of the hyperfine field of the nuclear spins is sketched in figure 2.2. It constitutes the fastest contribution to hyperfine-related electron spin depolarization with a time constant in the nanosecond range.[24]

Additionally, also the effective magnetic field of spin polarized electrons $\vec{B}_e \propto -A_n |\Psi(\vec{r}_n)|^2 \vec{s}$ will affect the nuclear spins. This Knight field is spatially inhomogeneous, as it depends on the value of the electron wavefunction at each nucleus' position. Consequently, the precession of the nuclear spins around \vec{B}_e will not be synchronized over the whole QD, which contributes a further stage to the spin dephasing process with a longer time constant. As the electron spin will follow the resulting change in the orientation of $\delta\vec{B}_N$, the behaviour gets rather complex. Typ-

ically, this mechanism will decrease the remaining electron spin polarization along the initial direction by another factor of three to four.[24]

The third stage of hyperfine-related electron spin depolarization is then related to the nuclear spin relaxation, typically dominated by dipole-dipole interactions. This mechanism is not conserving total spin and thus leads to complete spin relaxation. The corresponding time constant is rather long, though, and can reach up to seconds.[33]

2.4 Dynamic nuclear polarization

The dynamic effect of the hyperfine interaction on the nuclear spin ensemble provides the possibility to dynamically polarize the nuclear spins. As already mentioned, a sizeable equilibrium polarization of the nuclear spins is difficult to achieve in typical static external magnetic field strengths and at standard low temperatures, due to the small value of the nuclear magnetic moment. However, using the transfer of angular momentum from electrons to the nuclei via the hyperfine interaction (spin flip-flops), high polarization degrees of the nuclear spins can be achieved. Continuous excitation of oriented electron spins by circularly polarized light and subsequent spin flip-flops with the nuclear spins will lead to accumulation of nuclear spins (dynamic nuclear polarization, DNP) along the electron spin direction, as the longitudinal nuclear spin relaxation due to dipole-dipole interactions is slow and may be further suppressed by very small external magnetic fields.[33] It is actually the Knight field of the electron spin itself, that, by suppressing the nuclear spin dipole-dipole interactions, enables the DNP build-up in zero external magnetic field in the first place.[34]

It should be noted, that the generation of DNP leads in turn to an increase in electron Zeeman spin splitting due to its effective hyperfine field. An increase in the electron spin splitting will decrease the efficiency of further build-up of DNP due to the increasing energy mismatch between the electron and nuclear spin levels.[35] This feedback restricts the magnitude of DNP at low temperatures.

Experimentally, the contribution of DNP in an optical measurement can be controlled by using excitation light of constant helicity only, e.g. σ^+ , where DNP is possible, or by alternating the light helicity at high frequency using a PEM, see section 3.3. The time constant for the build-up of DNP has been found to be in the

range of milliseconds[33], so that the 50 kHz frequency of a typical PEM is sufficient to suppress DNP.

2.5 Effects of external magnetic fields

2.5.1 Landau levels

Electrons moving with velocity \vec{v} in a static uniform magnetic field $\vec{B} = (0, 0, B_z)$ will experience a Lorentz force $\vec{F}_L = e\vec{v} \times \vec{B}$, which will result in a circular motion of the electron in the plane perpendicular to \vec{B} , i.e. the x - y -plane. The electron motion along the \vec{B} -field direction stays unaffected. The Hamiltonian for this system is thus separable into these two components. The magnetically induced confinement of electron motion in the x - y -plane leads to a set of discrete states, the Landau levels (LL), similar to the eigenstates of a simple one-dimensional harmonic oscillator, with the following energies:

$$E_n = \left(n + \frac{1}{2} \right) \hbar\omega_c \quad (2.1)$$

The resonant frequency $\omega_c = eB_z/m^*$ is the cyclotron frequency, where e is the absolute value of the electron charge and m^* its effective mass. The z -component of electron motion adds a parabolic $E(\vec{k})$ term for each of the above discrete orbits in the x - y -plane.

For carriers in a two-dimensional system, e.g. in a WL, exposed to a longitudinal magnetic field, i.e. \vec{B} parallel to the growth and confinement direction, the z -motion is hindered by the quantum confinement. Thus the corresponding $E(\vec{k})$ continuum is suppressed and we can expect discrete LL states following eq. (2.1).

Optical excitation is now only possible from an occupied VB LL to an empty CB LL. Thus the optical transition energy will change with the sum of the individual cyclotron frequencies. This corresponds to a replacement of the single-carrier effective mass m^* by the reduced effective mass μ of the electron-hole pair with $1/\mu = 1/m_e + 1/m_h$ in the relation for the cyclotron frequency above.

For quantum confined electron-hole pairs, exciton formation will affect the magnetic field dependence of their energy position.[36] Two magnetic field ranges can be distinguished: the low-field range, where the cyclotron energy $E_c = \hbar\omega_c$ is smaller

than the exciton binding energy, $E_c < E_b$, and the high-field range, where the cyclotron energy is larger than the exciton binding energy, $E_c > E_b$.

In the low-field range the exciton level shows a quadratic, diamagnetic energy shift with B . In the high-field range, the cyclotron motion dominates and leads to separate LL for electrons and holes. These states experience then electron-hole-coupling, shifting their energies with only a small square-root dependence on B in addition to the general linear LL shift. The transition from the low-field to the high-field range has been found to occur in the range of around 9 T for self-assembled InGaAs/InP QDs.[36]

2.5.2 Zeeman splitting

The previous discussion only considered the effect of a magnetic field on the electron motion, seen as a moving charge. However, the magnetic field will also interact with the magnetic momenta of the electron, resulting in a spin splitting of the electronic levels.

Similarly to the magnetic moment of a current loop $\vec{\mu} = I\vec{A}$, which is proportional to the current I and the enclosed area \vec{A} , also an electron circling around the nucleus has a magnetic moment. The electron's magnetic moment consists of two contributions, though. One is proportional to its orbital angular momentum $\vec{\mu}_l = -\mu_B\vec{l}/\hbar$ and the other one is related to its spin $\vec{\mu}_s = -g\mu_B\vec{s}/\hbar$. The proportionality constant μ_B is the Bohr magneton and g the Landé g -factor. For a free electron $g \approx 2$, whereas for electrons in solids the spin-orbit interaction may result in rather large deviations from this value.

In an external magnetic field \vec{B} , the interaction of the electron's magnetic moment with \vec{B} results in a potential energy change by the amount $-\vec{\mu} \cdot \vec{B}$. In the general case of non-zero spin and orbital angular momentum, the spin-orbit interaction between these two results in the fact, that the potential energy is determined by the total angular momentum as a whole $-\vec{\mu}_j \cdot \vec{B}$ (in weak magnetic fields). So the energies of the electronic states are determined by the values j_z of the total angular momentum. For s-type CB electrons, where $l = 0$, this effectively is a spin-splitting. The two spin orientations result in an energy level shift by the energy

$$E_z = g\mu_B(\vec{s} \cdot \vec{B}). \quad (2.2)$$

Thus, the total splitting between a spin-up $s_z = 1/2$ and a spin-down $s_z = -1/2$ CB state in a collinear magnetic field $\vec{B} = (0, 0, B_z)$ is the Zeeman splitting $\Delta E_Z = g_{CB}\mu_B B_z$. For the hh VB states, the Zeeman splitting is accordingly $\Delta E_Z = 3g_{VB}\mu_B B_z$, as here $j_z = \pm 3/2$.

2.5.3 Spin polarization in a longitudinal magnetic field

Optical measurements of spin properties in epitaxial nanostructures are usually done under excitation and detection along the sample growth direction, perpendicular to the sample surface. As this is the direction of the strongest quantum confinement, this also determines the direction along which the spin is well defined.

Applying an external magnetic field along the growth direction can result in several effects, which will be discussed with reference to the structures investigated in this thesis. As shown in the previous subsections, LL will be formed at high fields both in the GaAs barrier and the WL. These LL may in addition show a Zeeman spin splitting due to the splitting of the single electron and hole levels. In the QD itself only a Zeeman splitting of the excitonic states is significant. The occurrence of LL is not possible due to the discrete nature of the QD states from the start.

However, already at lower magnetic fields, the spin polarization inside the QDs can be strongly affected by the suppression of the spin depolarization mechanisms discussed in sections 2.3.1 and 2.3.2, namely the AEI and the hyperfine interaction.

Anisotropic exchange interaction in a longitudinal magnetic field

AEI results in a splitting δ_1 of the QD bright excitonic ground state of a neutral exciton into two linearly polarized eigenstates $|X\rangle$ and $|Y\rangle$, see section 2.3.1. The action of this AEI can be seen as arising from an effective magnetic field in the plane of the QDs, the anisotropic exchange field. In a sufficiently strong external magnetic field along the z -direction, B_z , the effect of this AEI field will be very small and thus circular symmetry and circularly polarized eigenstates $|\pm 1\rangle$ will be restored. The change of the polarization degree with magnetic field can be described by [37; 38]:

$$P(B_z) = P_0 \frac{\Omega_z^2}{\Omega_z^2 + \omega_{AEI}^2} \quad (2.3)$$

where $\hbar\omega_{AEI} = \delta_1$ the AEI splitting, $\hbar\Omega_z = g^X\mu_B B_z$ the Zeeman-splitting with g^X the longitudinal exciton g -factor. P_0 is the saturation polarization degree at high

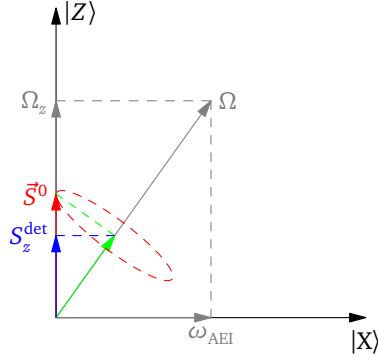


Figure 2.3: Schematic representation of the pseudospin model after [37]. The symbols are defined in the text.

magnetic fields. The mechanism can be described by a simple pseudospin model as shown in Figure 2.3. The AEI field, characterized by its zero-field splitting of the radiative double $\hbar\omega_{\text{AEI}}$, and the external longitudinal magnetic field, characterized by the spin precession frequency Ω_z , result in a total vector Ω , which is oblique. The excited spin vector \vec{S}^0 precesses around Ω . The precession preserves only the projection of \vec{S}^0 on Ω , shown as a green vector in the figure. The optical detection along the z -direction registers then the z -component of this projection S_z^{det} . For $B_z = \Omega_z = 0$, of course, $S_z^{\text{det}} = 0$. With increasing external magnetic field B_z , Ω_z will increase and thus the spin projection onto the z -axis. For strong magnetic fields, thus large Ω_z , no spin components will be lost and the detected polarization $P \rightarrow -2|\vec{S}^0|$. Experimentally, typical X^0 AEI splittings in the range of some tens of μeV have been found[24], reaching up to $150 \mu\text{eV}$ [27] in InAs/GaAs QDs.

As discussed before in section 2.2, singly charged excitonic complexes, e.g. X^+ , do not show such splitting and their ground states are spin pure. In an ensemble of QDs, containing both singly positive charged and neutral species, a certain circular polarization degree in zero external magnetic field should then be attributable to X^+ , whereas in strong magnetic fields B_z , both X^+ and X^0 will contribute to the circular polarization.

Hyperfine interaction in a longitudinal magnetic field

As discussed in subsection 2.3.2, randomly oriented nuclear spins interact with the electron spin and contribute to its dephasing via their hyperfine field. The physical

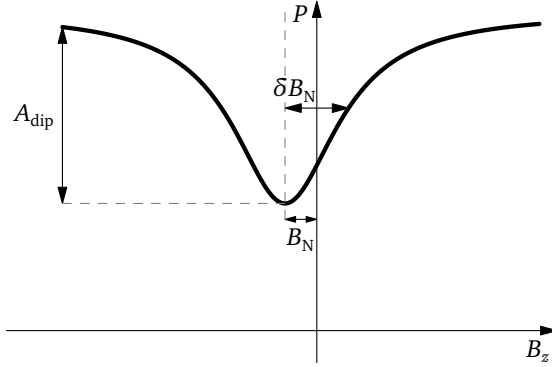


Figure 2.4: The effect of quenching the hyperfine induced electron spin dephasing on PL circular polarization degree in an external longitudinal magnetic field according to equation (2.4).

model is similar to the one above in the discussion of AEI. The in-plane components of the fluctuating nuclear field take over the role of the AEI field, leading to dephasing of the initially oriented spin ensemble due to their random orientation and strength over time and for different QDs in the ensemble. A Lorentzian dip shape of the polarization curve as a function of longitudinal magnetic field has been obtained theoretically in [31; 39].

The experimentally observed circular polarization degree P as a function of longitudinal magnetic field B_z is sketched in figure 2.4 and can be described by the following formula[32; 40]:

$$P(B_z) = P(\infty) \left(1 - \frac{A_{\text{dip}}}{1 + [(B_z + B_N)/\delta B_N]^2} \right) \quad (2.4)$$

Here, $P(\infty)$ denotes the polarization degree that can be reached in strong magnetic fields, when the dephasing mechanism is suppressed, and A_{dip} is the strength of the depolarization dip. It characterizes the extent of dephasing. The half-width δB_N of the dip characterizes the strength of the nuclear field fluctuations, which have been found to be in the range of a few tens of milli-Tesla[40; 41]. B_N accounts for a total shift of the dip due to the effective hyperfine field of the DNP which can build up under circularly polarized excitation of static helicity. The orientation of this effective magnetic field depends on the helicity of the excitation light and will thus shift the polarization dip away from zero field to the field magnitude and direction, where the external magnetic field B_z compensates the DNP field B_N . This provides a convenient way to measure both the magnitude and orientation of the DNP field. Typical DNP

field strengths in QD ensembles have been found to be in the range of some tens of milli-Tesla.[40]

2.5.4 Spin depolarization in a transverse magnetic field

The action of an external magnetic field in the plane perpendicular to the spin orientation, can be discussed using the scheme shown in figure 2.3, too. However, in the case of such a transverse field, no component Ω_z along the z -direction exists, so the initial spin vector is going to precess around the magnetic field direction, taken along the x -axis, solely. For sufficiently strong magnetic fields and sufficiently long lifetimes, this precession will of course result in complete dephasing of the electron spin ensemble, so no S_z^{det} can be observed in a continuous wave experiment. Time resolved measurements, however, have been able to show the precession directly as an oscillation in the circular polarization degree of the recombination luminescence.[42]

In continuous wave experiments, on the other hand, the steady state value of the polarization is measured. For the neutral exciton under conditions of no DNP, the polarization can be expected to be zero due to their fine-structure splitting. Only trions will contribute circular polarization. Their steady state polarization degree will be determined by the actual values of the precession frequency, which is dependent on the magnetic field, the spin relaxation time τ_s , as well as the lifetime τ of the trion. Both τ_s and τ enter the equation, as both events of spin relaxation or carrier recombination/reemission will terminate the coherent spin precession.

From the simple equation of motion for the spin vector \vec{S} [30, Ch. 1]

$$\frac{d\vec{S}}{dt} = \vec{\Omega} \times \vec{S} - \frac{\vec{S}}{\tau_s} - \frac{\vec{S}}{\tau} + \frac{\vec{S}_0}{\tau} \quad (2.5)$$

where $\vec{\Omega} = g\mu_B\vec{B}/\hbar$ is the precession frequency and \vec{S}_0 is the generated spin by optical excitation, the dependence of the detected steady state spin component along the z -direction in a transverse magnetic field B_x , $S_z(B_x)$, can be obtained to

$$S_z(B_x) = \frac{S_z(0)}{1 + (\Omega_x T_s)^2} = \frac{S_z(0)}{1 + B_x^2/B_{1/2}^2} \quad (2.6)$$

Here the spin lifetime $T_s = 1/(1/\tau + 1/\tau_s)$ is introduced. As a function of B_x , this curve has the shape of a Lorentzian and can be rewritten directly in terms of the magnetic field, using the half-width field at half maximum (HWHM) $B_{1/2} = \hbar/g\mu_B T_s$, as given in the right hand side of equation (2.6). Such spin depolarization in a

transverse magnetic field is called Hanle effect as it has been described initially for the depolarization of resonantly excited fluorescence of atomic gases by Hanle[43].

For measurements on the emission line of a positive trion X^+ in single QDs at low temperature[44], the Hanle curve has been attributed to the electron lifetime τ , limited by radiative recombination. The data from negatively charged trions X^- , however, showed an extremely sharp Hanle curve, corresponding to a very long T_s , exceeding reasonable values for both lifetime and spin relaxation time of the hole in the trion, which determines the observed polarization degree at the moment of recombination. Consequently, it has been attributed to the resident electron, left behind after recombination of an electron-hole pair from the trion. The depolarization mechanism here is the dephasing of the electron spin in the random fluctuations of the hyperfine field of the nuclei,[45] which will be discussed in the following.

The above derivation of the Hanle curve formula considered only single spins, or at least identical ensembles. Self-assembled semiconductor QDs are, however, inherently inhomogeneous, meaning, that their size and shape differ from dot to dot. Thus the local environment for each electron spin will be slightly different, leading to different precession frequencies $\vec{\Omega}$. Experimental observation of the polarization from many QDs will thus show an additional effect of ensemble dephasing, leading to a loss of polarization characterized by the ensemble dephasing time T_2^* . In the formula for the Hanle effect, this can be accounted for by letting $1/\tau_s = 1/T_1 + 1/T_2^*$.

One possible mechanism for such dephasing is the previously mentioned random fluctuations of the hyperfine field of the QD nuclear spins δB_N , see section 2.3.2. Their effect in external magnetic fields has been described theoretically in [31]. If the coherence time of the electron-nuclear spin interaction, i.e. both the lifetime τ and spin relaxation time τ_s , is sufficiently long, then the electron spin depolarization, and consequently also the Hanle curve width in equation 2.6, is dominated by the dephasing time T_2^* . This consideration has led to the attribution of the experimentally observed X^- Hanle curves to the dephasing of the resident electrons' spins.[45; 46] A further ensemble effect, the dispersion of g-factors in the QD ensemble, has also been discussed. With increasing magnetic field strength, the individual spin precession frequencies will spread more and more, contributing a spin dephasing, which can even lead to a change in the Hanle line shape from Lorentzian to Gaussian for large dispersions.[47]

Furthermore, Hanle curves have been found to consist of several Lorentzian lines,

indicating a contribution from different spin species.[46] Apart from the spin dephasing of the resident electrons discussed above, their characteristic time constants have often been found too short to match any of the lifetimes or spin relaxation/dephasing times determined by other experimental means for relevant carriers and carrier pairs in the ground state of typical III-V based QDs.[45; 48] Thus they have been attributed to the depolarization of the carriers during their capture and relaxation stages into the QD ground state, consistent with the evolution of polarization in time-resolved PL data.[49] On the other hand, in II-VI QDs, e.g. in the CdSe/ZnSe system, where the polarization is known to be dominated by negatively charged trions, the obtained Hanle curves have shown widths consistent with an interpretation as arising from the depolarization of holes in the X^- trions, limited by their radiative lifetime.[50]

2.6 Effects of elevated temperatures

When raising the sample temperature, an increase in phonon density typically starts to affect the spin polarization degree in the QDs by providing scattering events that can relax the spins. Thus a decreasing polarization degree is to be expected with rising temperature. The carrier concentration itself in the QD is typically much less affected initially, as the carriers do not escape from the QD due to the strong confinement and the absence of non-radiative recombination centers in the QDs because of their small size.

The dependence of the QD PL intensity I as a function of temperature T can be used to investigate thermal activation mechanisms for the PL quenching and to extract their activation energies. The intensity is assumed to follow

$$I(T) = \frac{I_0}{1 + A \exp\left(-\frac{E_a}{k_B T}\right)} \quad (2.7)$$

for a single thermal activation mechanism, where I_0 is the low temperature value of the PL intensity, A a constant containing the density of states in both the initial and final level, E_a the thermal activation energy and k_B the Boltzmann constant. In a plot of the logarithm of the intensity over reciprocal temperature, called the Arrhenius plot, a linear dependence should be reached where the slope E_a/k_B gives the activation energy.

In the literature, activation energies deduced by this procedure have been attributed to a variety of final states, being either excited QD states, WL or barrier states, and mechanisms, being either emission of single carriers, excitons or correlated electron-hole pairs. A recent survey over relevant publications can be found in [51]. It is furthermore shown, that carrier transport in the WL and retrapping to the QDs may mask the actual activation energy of the dominating thermal activation process, further complicating the interpretation of such data.

The decreasing spin polarization in QDs with rising temperature[52; 53] has been ascribed to an increasing phonon scattering.[54; 55] As phonons do not couple to the spin directly, an additional spin coupling is necessary, typically via the spin-orbit coupling, to achieve a spin flip during the scattering. These mechanisms are dominant in the temperature range of several tens of K, where the carrier lifetime is still unaffected.

The complex interaction of the electron spin with the QD nuclei has recently been reported to result in an interesting effect, namely that the DNP increases with temperature, despite an overall decrease in electron spin polarization and electron spin relaxation time.[56] These experiments have been conducted in an external magnetic field, resulting in a Zeeman splitting of the electron levels that limits the DNP efficiency at low temperatures. The proposed explanation is thus based on a spin level broadening with rising temperature that simplifies the electron-nuclear spin flip-flops.

An increase in phonon-mediated spin depolarization has also been given as the cause for a broadening of the Hanle components with temperature, as their width scales inversely with the respective spin depolarization time constants.[45; 49] The decreasing electron spin polarization is reflected by a decrease in the magnitude of the respective Hanle components.[45; 46; 49; 57] For the broadest Hanle component, however, a rather temperature independent behaviour has been reported.[46; 57]

In this chapter the applied experimental methods and some corresponding background information are given. First, some important aspects of light and its application in photoluminescence experiments are discussed, followed by a description of the working principle of polarization optics. Finally, the optical orientation method will be summarized and an overview picture over optical measurements on QD structures will be given.

3.1 Light

In everyday-life, (visible) light is probably most often regarded as an electromagnetic wave, characterized by a certain wavelength λ . Both electric and magnetic field vectors vary sinusoidally in space and time and are orthogonal at all times. As the speed of propagation of light c is constant in a given material, each wavelength is uniquely connected to a frequency $\nu = c/\lambda$. The wave properties of light are described by Maxwell's equations and are able to explain characteristic phenomena like interference.

On the other hand, many experiments using light can only be explained by assuming particle-like properties of the light, e.g. the external photoelectric effect. These mass-less particles are called photons and their energy E is directly proportional to the frequency of the corresponding wave $E = h\nu$, where the proportionality constant h is the most fundamental quantum mechanical constant, Planck's constant.

The particle-wave-duality is also expressed in the relation $p = h/\lambda$, connecting the photon's linear momentum p to its de-Broglie-wavelength λ . But besides their linear momentum, photons also exhibit an angular momentum of $\pm\hbar = \pm h/2\pi$ along the direction of propagation, similar to electrons. These two orientations of the photon's angular momentum are referred to as circular polarization states, denoted by σ^+ and σ^- , respectively.

From the wave point of view, the circular polarization state corresponds to a continuous rotation of the electric (and thus also the magnetic) field vector around the propagation vector. The state of polarization where the electric field vector oscillates in only one direction at all times is called linearly polarized and may be denoted by σ^x .

Upon absorption of light by electrons in atoms (or matter in general), both energy and angular momentum will be transferred to it. In a first approximation, the energy

will determine to which shell of the atom the electron will be excited and the angular momentum of the photon will determine which specific subshell the electron will occupy. The angular momentum conservation law is the cause for the occurrence of selection rules. If the absorbed light carries angular momentum, then the absorbing electrons have to change their angular momenta accordingly. A more accurate description appropriate for light absorption in semiconductors will be given in section 3.6.

3.2 Photoluminescence

Photoluminescence (PL) experiments study the light (luminescence) emitted from a sample under optical excitation, which may be provided by a laser. A typical setup is depicted in Figure 3.1. In the following, the components will be described briefly.

In this thesis, mainly a tunable Ti:sapphire laser was used as the excitation light source. It consists of the titanium-doped sapphire (Al_2O_3) crystal within a laser cavity, which is pumped by a solid state laser emitting green light at a wavelength of 532 nm. This light pumps electrons in the Ti^{3+} ions into higher vibrational levels of an excited state from where they relax to lower levels. From these, lasing occurs through a transition into the ground state. As the states are vibrationally broadened, both absorption and emission may occur in a rather wide wavelength range. By tuning the Ti:sapphire laser cavity to amplify only one certain wavelength of the emission band, which is done by adjusting the angular position of a birefringent filter, laser action can be induced at this specific wavelength only. Continuous rotation of the birefringent filter will shift the laser wavelength through the emission band of the Ti:sapphire crystal, thereby enabling continuous tuning of the laser output wavelength over a wavelength range from around 700 nm to above 1000 nm.

The laser beam is mechanically blocked and admitted by a rotating chopper wheel at a frequency of typically around 200 Hz. A standard Lock-In amplifier then extracts the detector signal at this frequency, which yields the pure PL signal, where noise and background contributions with different characteristic frequencies are strongly suppressed.

A focusing lens in front of the sample focuses the excitation laser beam to a small spot, which increases the excitation power density. Inside the sample material, the laser light may be absorbed by different mechanisms. Some of them may eventually

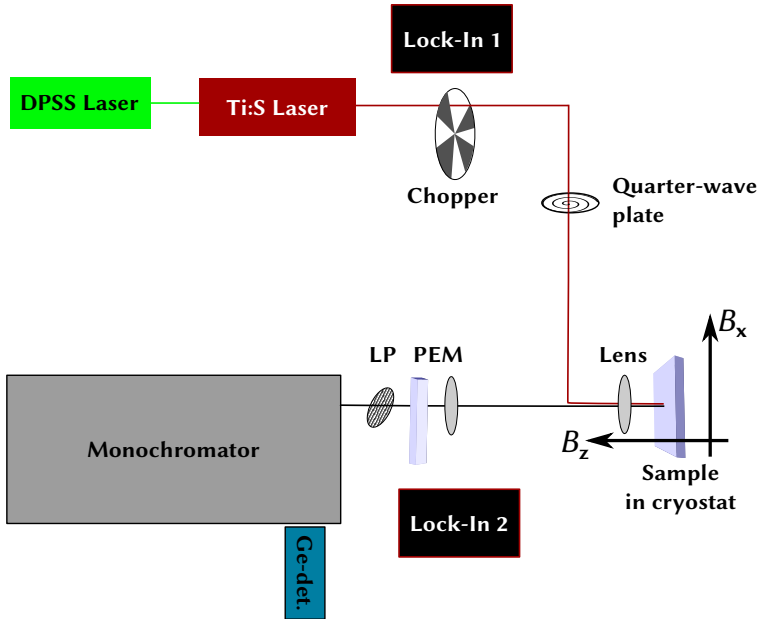


Figure 3.1: A typical polarized PL setup containing a pumped Ti:Sapphire laser, a chopper, a wave plate, lenses, the sample in a cryostat equipped with a magnetic field coil, a photoelastic modulator (PEM), a linear polarizer (LP) and a monochromator, connected to a Germanium-detector. Also two Lock-Ins are shown that analyze the detector signal at the respective frequencies of the chopper and the PEM. Thin lines give the path of light. For clarity, all cabling and mirrors are omitted.

result in the emission of light again. This luminescence light is collected again by the same lens and focused onto an entrance slit of a spectrometer by a second lens.

Inside the spectrometer, diffraction gratings disperse the incoming light spectrally. A single wavelength is selected by the output slit just in front of the detector. Liquid nitrogen cooled Ge-diodes have been predominantly used as detectors, as the luminescence of typical InAs-based QDs lies in the near infrared part of the electromagnetic spectrum. Only for some samples, emitting at wavelengths closest to the visible spectral range, it was possible to use a Si-based liquid nitrogen cooled charge coupled device (CCD) camera to collect the signal. Cooling of both detector types is necessary to reduce electrical noise inside the detector, caused by thermal activation of charge carriers. This noise would dominate over the PL-induced detector signal at room temperature.

For PL experiments at temperatures below room temperature, the sample was mounted on a sample holder, which was inserted into the sample space of a liquid-Helium bath cryostat. A connection of the sample space to a reservoir of liquid Helium (being at a temperature of 4.2 K) allows then cooling of the sample. An integrated heater in the sample space and a temperature sensor on a sample rod provides precise temperature control for temperatures between 4.2 K and 300 K.

Application of magnetic fields inside the cryostat was possible, as the cryostat was equipped with superconducting coils, that reside in the liquid Helium reservoir. Depending on the orientation of the sample, the magnetic field lines were either perpendicular (Faraday geometry) or parallel to the sample surface (Voigt geometry). Optical excitation and detection were always carried out perpendicular to the sample surface.

3.3 Polarization optics

To control the polarization state of the exciting laser beam and to analyse the polarization state of the luminescence polarization optics, such as linear polarizers and retarding wave plates were used.

Single mode laser light is linearly polarized, as all the radiating dipoles of the lasing medium are forced to emit with the same orientation in the process of stimulated emission. During reflection from the mirrors that guide the laser beam to the sample, this perfect linear polarization may sometimes be affected. To establish a fixed linear polarization orientation, a linear polarizer is typically used, followed by a rotatable broadband quarter-wave plate, that allows conversion of linearly polarized light into circularly polarized light.

A quarter-wave plate consists of a birefringent crystal (e.g. Calcite) of a specific thickness and crystalline orientation. In a birefringent material a preferential crystalline symmetry axis exists, which has no equivalent axis in the plane perpendicular to it. Light, which is polarized along this extraordinary (or "optical") axis will experience a different refractive index n than light which is polarized perpendicular to it (along the ordinary axis). The difference in refractive indices for the two polarization directions will result in a different speed of light through the crystal for the two polarization states, as $c = c_{\text{vac}}/n$ (where c_{vac} is the speed of light in vacuum). So if the incoming linearly polarized laser beam travels perpendicular to the optical axis

with its polarization oriented at 45° to it, it will be split up into two perpendicularly polarized components (being polarized along and perpendicular to the optical axis, respectively) which travel at different speed through the crystal. If now the thickness of the crystal is properly chosen such that the phase difference between these two components corresponds to one quarter of a full cycle, then the coherent interference of these two beams after the crystal will produce circularly polarized light. The resulting electric field vector at the output surface of the crystal will rotate from the fast axis towards the slow axis and so on. The orientation of this circularly polarized light (being right-handed or left-handed) can be chosen by orienting the optical axis at either $+45^\circ$ or -45° to the incoming linear polarization. If the optical axis is parallel to the incoming linearly polarized electric field vector (corresponding to 0° orientation of the quarter-wave plate) then the incoming beam will not be split up and just pass the crystal without any polarization change, being still linearly polarized after it. Thus a simple rotation of the quarter-wave plate between the three positions $\pm 45^\circ$ and 0° allows choosing the excitation polarization between both circular orientations and one linear orientation, respectively.

A quarter-wave plate can as well be used to convert circularly polarized light back into linearly polarized one. As σ^+ and σ^- polarized light will be converted into two perpendicular linear polarization components after having passed the quarter-wave plate, a following linear polarizer can selectively suppress one of them, making it possible to e.g. analyse the circular polarization degree of the sample luminescence by recording the two polarization components separately.

Some crystals (e.g. fused silica) show birefringence only under application of mechanical stress (the photoelastic effect). When such a crystal is periodically compressed and extended (most efficiently at its mechanical resonance frequency), also its birefringence oscillates. This can be used like a quarter-wave plate that oscillates rapidly between $+45^\circ$ and -45° . Thus, in conjunction with a linear polarizer, such a photoelastic modulator (PEM) can be used to extract the difference between the two circular polarization components of the detected luminescence at the oscillation frequency from a single measurement using a second Lock-In amplifier.

Like this it is possible to extract both PL intensity and its polarization degree from a single measurement when using two Lock-In amplifiers that extract the signal amplitudes at the two frequencies - the PL intensity at the lower frequency of the mechanical chopper and the polarization signal at the PEM's frequency (50 kHz).

The polarization degree of a luminescence signal P is generally defined as the difference between the intensities of the two opposite polarization components (e.g. I^{σ^+} and I^{σ^-}) divided by the total signal:

$$P = \frac{I^{\sigma^+} - I^{\sigma^-}}{I^{\sigma^+} + I^{\sigma^-}} \quad (3.1)$$

In the case of measurements using static quarter-wave plates, I^{σ^+} and I^{σ^-} are detected when rotating the quarter-wave plate to $+45^\circ$ and -45° , respectively. Thus two measurements are needed to calculate the polarization degree P . When using the PEM, the difference between the two polarization components $I^{\text{PEM}} = I^{\sigma^+} - I^{\sigma^-}$ is obtained at the PEM frequency, whereas the average between them $I^{\text{ch}} = (I^{\sigma^+} + I^{\sigma^-})/2$ is obtained at the chopper frequency from a single measurement. As a correct measurement at the high PEM frequency is sometimes hindered by an insufficient time constant of the whole detection system, such a setup needs careful calibration using a known polarization source.

3.4 Photoluminescence of semiconductors

When an excitation laser beam of sufficient photon energy hits a semiconductor sample, the photon's energy can be absorbed by an electron in the VB, which is then excited into empty states in the CB, leaving behind a hole in the VB. In a first stage, the electron and hole will typically relax their excess energy and momentum by interaction with phonons or other carriers to reach the CB minimum and VB maximum, respectively. From there, they may either recombine radiatively, i.e. the electron relaxes back into the VB with emission of a photon, or they may get captured into states of lower energy, such as excitonic states, single carrier states at defects or states in another part of a heterostructure. For many defects, the capture of carriers happens non-radiatively, i.e. without creation of photons, which makes these transitions invisible in PL measurements.

Observing a PL signal, only the radiatively recombining portions of electrons and holes are monitored. Thus, information about the band structure, excitonic properties and some particular defects can be obtained, where electrons and holes can recombine radiatively. Only indirectly, i.e. via a change in the luminescence of another transition, also non-radiative channels may be evidenced.

In the PL spectra of QDs under high excitation power density, typically several broad peaks are observed, as shown in the right part of figure 3.2. They originate from recombination in the discrete states of the QD, broadened by the distribution of the energy levels in the inhomogeneous QD ensemble.

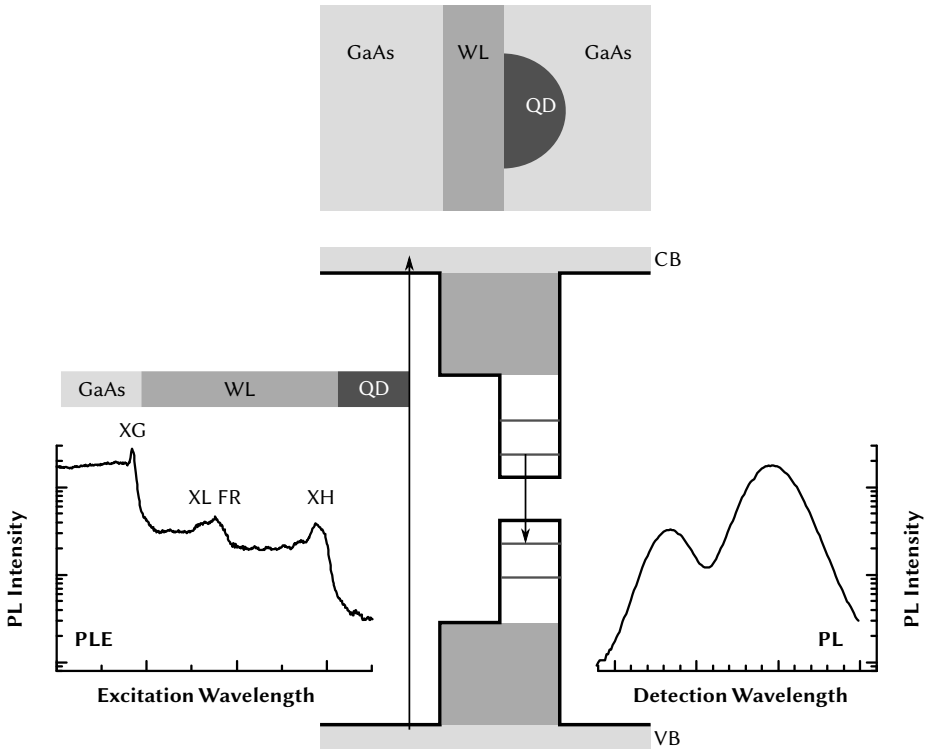


Figure 3.2: An overview picture over the structure (top), band structure (center) and PL (right) as well as PLE (left) spectra of a typical self-assembled QD sample. The abbreviations are discussed in the text.

3.5 Photoluminescence excitation spectroscopy

In PL excitation spectroscopy (PLE), the PL intensity at a fixed wavelength is monitored while the excitation energy is scanned in a certain range. Thus the efficiency of absorption and carrier relaxation and/or transport to the final state, from which the PL intensity is monitored, can be characterized as a function of excitation energy.

In the QD structures investigated in this thesis, three different sample regions can be distinguished in the order of higher to lower energy states: the GaAs, the InAs WL and the InAs QDs. They are shown schematically in the top part of figure 3.2. Electrons and holes created by photon absorption in the GaAs barriers may be captured into either the InAs WL and then relax further into the QDs or they may be captured directly by the InAs QDs. On the other hand, excitation at an energy below the GaAs bandgap only allows creation of electrons and holes in the WL and the QDs. Lowering the excitation energy further, below the WL bandgap, carriers may only be excited directly within the QDs or via cross-transitions from the QD hole states to the WL CB or from the WL VB to the QD electron states. A sketch of the band structure is given in the center of figure 3.2. For each step in excitation energy, the absorption efficiency decreases strongly, as the volume and thus the density of states that is available for absorbing the photons decreases from the three-dimensional GaAs barrier to the thin two-dimensional WL and further to the zero-dimensional QDs.

When tuning the Ti:sapphire laser's photon energy through these three ranges, a distinct step-like shape is obtained, which is mainly related to the absorption efficiency. The observed absorption steps facilitate the identification of the three energy ranges and enable one to address them separately, studying their injection behaviour into the QDs, from which the luminescence is monitored. A typical PLE spectrum of the QD ground state PL intensity is shown in the left part of figure 3.2. The three regions are identified in the shaded areas above the spectrum.

In addition to these band-to-band (BB) transitions, creating free electrons and free holes in the respective CB and VB, also free excitons may be created at energies slightly below the onset of the respective BB transitions. Such excitonic transitions show up as inhomogeneously broadened peaks, due to their relatively high density of states. In the PLE spectrum in figure 3.2, the GaAs free exciton (XG), the Fano resonance at the lh exciton in the WL (XL FR) and the hh exciton XH are identified.

3.6 Optical Orientation

As discussed in section 2.1, due to spin-orbit interaction, the VB holes are characterized by the quantum numbers for their total angular momentum j and its projection on a preferential axis, j_z .

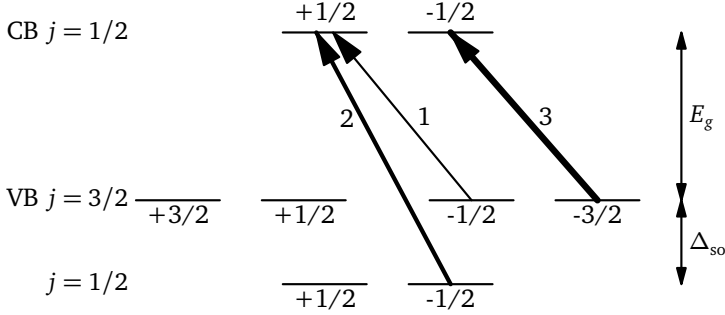


Figure 3.3: Energy level scheme at the band edges of an unstrained cubic semiconductor. The given levels are labelled by the projection of their total angular momentum j_z . Band-to-band transitions that are allowed for σ^+ polarized excitation are indicated by arrows. Their relative oscillator strengths are given by the numbers on the arrows.

Under excitation by circularly polarized light, the photon's angular momentum of ± 1 is transferred to an electron that is excited from the VB to the CB. This requirement of angular momentum conservation leads to selection rules, which forbid certain transitions from some of the VB states into the CB states. Figure 3.3 shows the allowed transitions for a σ^+ polarized photon.

Transitions to the spin-down state \downarrow in the CB, $j_z = -1/2$, are only possible from the hh VB for the $j_z = -3/2$ state. Spin-up \uparrow electrons can be excited from both the lh VB state $j = 3/2, j_z = -1/2$ and the $j = 1/2, j_z = -1/2$ state of the spin-orbit split-off VB. The relative oscillator strengths of these transitions are 3:1:2.

The spin-orbit splitting Δ_{so} opens a way to create a preferential spin orientation in the CB, by exciting with a photon energy lying between E_g and $E_g + \Delta_{so}$. Due to the difference in the relative oscillator strengths of the respective VB-CB transitions a CB electron spin polarization of $\rho = \frac{3-1}{3+1} = 0.5$ will result. This technique of orienting an electron spin population by optical excitation using circularly polarized light is called optical orientation and constitutes the experimental basis of the work presented in this thesis. The efficiency of optical orientation will be improved further in quantum confined and/or strained structures where the hh and lh VB are split and a single transition from e.g. the hh VB states can be addressed selectively.

4 Summary of Papers

A clear difference in the efficiency of spin generation and injection under excitation of pairs of uncorrelated free carriers from WL band-to-band transitions vs. creation of excitonic correlated carrier pairs has been found and investigated in **papers 1** and **2**. A reduced spin polarization in the QD ground state upon generation of spin-oriented hh excitons (XH) from the WL has been ascribed to the accelerating spin relaxation caused by the electron-hole Coulomb exchange interaction in the exciton before reaching the QD ground state. This effect has been shown to be relevant up to elevated temperatures and has been confirmed to be unrelated to the differing QD carrier densities created under these two conditions during a standard constant-excitation-power PLE scan. Injection of separate, uncorrelated, carriers, as is employed in electrical spin injection devices, has thus been shown to be advantageous for spin conserving transport.

In **paper 3** a very efficient suppression of spin generation at the lh excitonic resonance XL in the WL of a variety of InAs/GaAs QD structures is shown. Strong spin scattering promoted by the Fano resonance (FR) between the discrete excitonic transition XL and the overlapping continuum of hh-e transitions under the influence of the electron-hole Coulomb exchange interaction and hh-lh scattering/mixing is proposed as the underlying mechanism, leading to a complete randomization of the excited carrier spins. The complete suppression of spin orientation is found to be rather robust, being present in different sample structures and also stable for temperatures exceeding 100 K. The results suggest that spin generation and injection via a FR at the XL are disadvantageous. The close energetic vicinity to the range of efficient spin generation from the hh-e continuum transitions may open the possibility of simple high-contrast modulation of spin generation by tuning the XL FR in and out of resonance with optical or electrical pumping, e.g. by employing electrical fields to Stark-shift the XL resonance.

In **paper 4**, the effects of a longitudinal magnetic field on optical spin generation, relaxation and detection in the WL and QDs, respectively, are studied for different sample structures. The ensemble QD spin detection efficiency has been found to increase by a factor of up to 2.5 in magnetic fields up to 2 T, which could be attributed to a suppression of spin depolarization mechanisms within the QDs, such as hyperfine interaction with the random correlations of the nuclear spin system and anisotropic electron-hole exchange interaction. At higher magnetic fields, structures showing in-plane strain anisotropy in the WL, such as laterally aligned double QDs, still show a

rather strong, linear, magnetic field dependence of their QD spin polarization under non-resonant excitation. This is ascribed to stronger spin relaxation of the carriers in the spin injector (WL or GaAs barrier) before their capture into the QDs, consistent with the lower overall spin injection efficiency in these structures at zero magnetic field.

In **paper 5**, electron spin dephasing and relaxation due to hyperfine interaction with the nuclear spin system is studied as a function of temperature. The efficiency of dynamic nuclear polarization generation is found to increase with temperature up to 85 K, limited by the detection sensitivity of the applied method. At the same time, the extent of hyperfine-induced spin dephasing reduces with temperature. Both effects are attributed to an accelerating electron spin relaxation through phonon-assisted electron-nuclear spin flip-flops driven by the hyperfine interaction. It is suggested, that this mechanism could become the main contribution to electron spin depolarization at elevated temperatures.

At temperatures reaching up to room temperature, a surprising sharp rise in the QD polarization degree with increasing temperature has been reported in **paper 6**, reaching 35% at room temperature, the highest value reported to date in QDs. The polarization increase is suggested to be contributed by a shortening of the carrier lifetime, restricting the extent of spin relaxation. In **paper 7** the first Hanle measurements, i.e. the spin depolarization curves in a transverse magnetic field, at temperatures approaching room temperature are presented. A constant width of the Hanle curve is interpreted as a constant electron spin dephasing time in the QD trion, which provided a bound on the trion lifetime at room temperature. It is concluded, that the polarization increase with temperature is due to both an increase in spin detection efficiency in the QD but also an increase in spin injection efficiency from the WL.

References

- 1 <http://commons.wikimedia.org/wiki/File:Sphalerite-unit-cell-depth-fade-3D-balls.png> (accessed 2011-10-02).
- 2 I. Vurgaftman, J. R. Meyer, L. R. Ram Mohan. Band parameters for III–V compound semiconductors and their alloys. *J. Appl. Phys.* **89** (2001) 5815–5875.
- 3 <http://commons.wikimedia.org/wiki/File:Stranski-Krastanow-Modus.svg> (accessed 2012-01-04).
- 4 P. W. Fry, I. E. Itskevich, D. J. Mowbray, M. S. Skolnick, J. J. Finley, J. A. Barker, E. P. O'Reilly, L. R. Wilson, I. A. Larkin, P. A. Maksym, M. Hopkinson, M. Al Khafaji, J. P. R. David, A. G. Cullis, G. Hill, J. C. Clark. Inverted Electron-Hole Alignment in InAs-GaAs Self-Assembled Quantum Dots. *Phys. Rev. Lett.* **84** (2000) 733–736.
- 5 D. M. Bruls, J. W. A. M. Vugs, P. M. Koenraad, H. W. M. Salemink, J. H. Wolter, M. Hopkinson, M. S. Skolnick, Fei Long, S. P. A. Gill. Determination of the shape and indium distribution of low-growth-rate InAs quantum dots by cross-sectional scanning tunneling microscopy. *Appl. Phys. Lett.* **81** (2002) 1708–1710.
- 6 S. Suraprapapich, S. Panyakeow, C. W. Tu. Effect of arsenic species on the formation of (Ga)InAs nanostructures after partial capping and regrowth. *Appl. Phys. Lett.* **90** 183112.
- 7 S. Suraprapapich, Y. Shen, V. Odnoblyudov, Y. Fainman, S. Panyakeow, C. Tu. Self-assembled lateral Bi-quantum-dot molecule formation by gas-source molecular beam epitaxy. *J. Cryst. Growth* **301-302** (2007) 735–739.
- 8 D. Loss, D. P. DiVincenzo. Quantum computation with quantum dots. *Phys. Rev. A* **57** (1998) 120–126.
- 9 G. Burkard, H.-A. Engel, D. Loss. Spintronics and Quantum Dots for Quantum Computing and Quantum Communication. *Fortschr. Phys.* **48** (2000) 965–986.
- 10 O. Gywat, G. Burkard, D. Loss. Biexcitons in coupled quantum dots as a source of entangled photons. *Phys. Rev. B* **65** (2002) 205329.
- 11 U. Fano. Effects of Configuration Interaction on Intensities and Phase Shifts. *Phys. Rev.* **124** (1961) 1866–1878.
- 12 A. E. Miroshnichenko, S. Flach, Y. S. Kivshar. Fano resonances in nanoscale structures. *Rev. Mod. Phys.* **82** (2010) 2257–2298.
- 13 D. A. Broido, E. S. Koteles, C. Jagannath, J. Y. Chi. Resonance broadening of the light-hole exciton in GaAs/Al_xGa_{1-x}As quantum wells. *Phys. Rev. B* **37** (1988) 2725–2728.
- 14 D. Y. Oberli, G. Böhm, G. Weimann, J. A. Brum. Fano resonances in the excitation spectra of semiconductor quantum wells. *Phys. Rev. B* **49** (1994) 5757–5760.
- 15 H. Xu, W. Sheng. Discontinuity in the phase evolution of electron transport in a quantum channel with attached quantum dots. *Phys. Rev. B* **57** (1998) 11903–11906.

-
- 16 K. Kobayashi, H. Aikawa, S. Katsumoto, Y. Iye. Tuning of the Fano Effect through a Quantum Dot in an Aharonov-Bohm Interferometer. *Phys. Rev. Lett.* **88** (2002) 256806.
- 17 J. F. Song, Y. Ochiai, J. P. Bird. Fano resonances in open quantum dots and their application as spin filters. *Appl. Phys. Lett.* **82** (2003) 4561–4563.
- 18 M. Torio, K. Hallberg, S. Flach, A. Miroshnichenko, M. Titov. Spin filters with Fano dots. *Eur. Phys. J. B* **37** (2004) 399–403.
- 19 M. Lee, C. Bruder. Spin filter using a semiconductor quantum ring side coupled to a quantum wire. *Phys. Rev. B* **73** (2006) 085315.
- 20 I. A. Shelykh, N. G. Galkin. Fano and Breit-Wigner resonances in carrier transport through Datta and Das spin modulators. *Phys. Rev. B* **70** (2004) 205328.
- 21 P. A. Orellana, M. Amado, F. Domínguez Adame. Fano–Rashba effect in quantum dots. *Nanotechnology* **19** (2008) 195401.
- 22 D. Sánchez, L. Serra. Fano-Rashba effect in a quantum wire. *Phys. Rev. B* **74** (2006) 153313.
- 23 K. Gündoğdu, K. C. Hall, Thomas F. Boggess, D. G. Deppe, O. B. Shchekin. Efficient electron spin detection with positively charged quantum dots. *Appl. Phys. Lett.* **84** (2004) 2793–2795.
- 24 Michel I. Dyakonov (Editor). *Spin Physics in Semiconductors* (Springer Berlin Heidelberg, 2008).
- 25 M. Z. Maialle, E. A. de Andrada e Silva, L. J. Sham. Exciton spin dynamics in quantum wells. *Phys. Rev. B* **47** (1993) 15776–15788.
- 26 S. Goupalov, E. Ivchenko. Electron–hole long-range exchange interaction in semiconductor quantum dots. *J. Cryst. Growth* **184–185** (1998) 393 – 397.
- 27 M. Bayer, G. Ortner, O. Stern, A. Kuther, A. A. Gorbunov, A. Forchel, P. Hawrylak, S. Fafard, K. Hinzer, T. L. Reinecke, S. N. Walck, J. P. Reithmaier, F. Klopff, F. Schäfer. Fine structure of neutral and charged excitons in self-assembled In(Ga)As/(Al)GaAs quantum dots. *Phys. Rev. B* **65** (2002) 195315.
- 28 A. Högele, S. Seidl, M. Kroner, K. Karrai, R. J. Warburton, B. D. Gerardot, P. M. Petroff. Voltage-Controlled Optics of a Quantum Dot. *Phys. Rev. Lett.* **93** (2004) 217401.
- 29 P. Desfonds, B. Eble, F. Fras, C. Testelin, F. Bernardot, M. Chamarro, B. Urbaszek, T. Amand, X. Marie, J. M. Gerard, V. Thierry Mieg, A. Miard, A. Lemaitre. Electron and hole spin cooling efficiency in InAs quantum dots: The role of nuclear field. *Appl. Phys. Lett.* **96** 172108.
- 30 F. Meier, B. Zakharchenya (Editors). *Optical Orientation* (North-Holland, Amsterdam, 1984).
- 31 I. A. Merkulov, A. L. Efros, M. Rosen. Electron spin relaxation by nuclei in semiconductor quantum dots. *Phys. Rev. B* **65** (2002) 205309.

REFERENCES

- 32 M. Y. Petrov, I. V. Ignatiev, S. V. Poltavtsev, A. Greilich, A. Bauschulte, D. R. Yakovlev, M. Bayer. Effect of thermal annealing on the hyperfine interaction in InAs/GaAs quantum dots. *Phys. Rev. B* **78** (2008) 045315.
- 33 P. Maletinsky, A. Badolato, A. Imamoglu. Dynamics of Quantum Dot Nuclear Spin Polarization Controlled by a Single Electron. *Phys. Rev. Lett.* **99** 056804.
- 34 C. W. Lai, P. Maletinsky, A. Badolato, A. Imamoglu. Knight-Field-Enabled Nuclear Spin Polarization in Single Quantum Dots. *Phys. Rev. Lett.* **96** 167403.
- 35 B. Eble, O. Krebs, A. Lemaître, K. Kowalik, A. Kudelski, P. Voisin, B. Urbaszek, X. Marie, T. Amand. Dynamic nuclear polarization of a single charge-tunable InAs/GaAs quantum dot. *Phys. Rev. B* **74** 081306.
- 36 O. Jaschinski, M. Vergöhl, J. Schoenes, A. Schlachetzki, P. Bönsch. Observation of Landau levels and excitons at room temperature in $\text{In}_{0.53}\text{Ga}_{0.47}\text{As}/\text{InP}$ quantum wells. *Phys. Rev. B* **57** (1998) 13086–13093.
- 37 R. I. Dzhioev, H. M. Gibbs, E. L. Ivchenko, G. Khitrova, V. L. Korenev, M. N. Tkachuk, B. P. Zakharchenya. Determination of interface preference by observation of linear-to-circular polarization conversion under optical orientation of excitons in type-II GaAs/AlAs superlattices. *Phys. Rev. B* **56** (1997) 13405–13413.
- 38 R. Dzhioev, B. Zakharchenya, E. Ivchenko, V. Korenev, Y. Kusraev, N. Ledentsov, V. Ustinov, A. Zhukov, A. Tsatsul'nikov. Optical orientation and alignment of excitons in quantum dots. *Phys. Solid State* **40** (1998) 790–793.
- 39 Y. G. Semenov, K. W. Kim. Effect of an external magnetic field on electron-spin dephasing induced by hyperfine interaction in quantum dots. *Phys. Rev. B* **67** (2003) 073301.
- 40 R. V. Cherbunin, S. Y. Verbin, T. Auer, D. R. Yakovlev, D. Reuter, A. D. Wieck, I. Y. Gerlovin, I. V. Ignatiev, D. V. Vishnevsky, M. Bayer. Dynamics of the nuclear spin polarization by optically oriented electrons in a (In,Ga)As/GaAs quantum dot ensemble. *Phys. Rev. B* **80** (2009) 035326.
- 41 O. Krebs, B. Eble, A. Lemaître, P. Voisin, B. Urbaszek, T. Amand, X. Marie. Hyperfine interaction in InAs/GaAs self-assembled quantum dots: dynamical nuclear polarization versus spin relaxation. *C. R. Phys.* **9** (2008) 874–884.
- 42 M. Sénès, B. Urbaszek, X. Marie, T. Amand, J. Tribollet, F. Bernardot, C. Testelin, M. Chamarro, J.-M. Gérard. Exciton spin manipulation in InAs/GaAs quantum dots: Exchange interaction and magnetic field effects. *Phys. Rev. B* **71** 115334.
- 43 W. Hanle. Über magnetische Beeinflussung der Polarisation der Resonanzfluoreszenz. *Zeitschr. Phys. A* **30** (1924) 93–105.

-
- 44 A. S. Bracker, E. A. Stinaff, D. Gammon, M. E. Ware, J. G. Tischler, A. Shabaev, Al. L. Efros, D. Park, D. Gershoni, V. L. Korenev, I. A. Merkulov. Optical Pumping of the Electronic and Nuclear Spin of Single Charge-Tunable Quantum Dots. *Phys. Rev. Lett.* **94** 047402.
- 45 Y. Masumoto, S. Oguchi, B. Pal, M. Ikezawa. Spin dephasing of doped electrons in charge-tunable InP quantum dots: Hanle-effect measurements. *Phys. Rev. B* **74** (2006) 205332.
- 46 R. J. Epstein, D. T. Fuchs, W. V. Schoenfeld, P. M. Petroff, D. D. Awschalom. Hanle effect measurements of spin lifetimes in InAs self-assembled quantum dots. *Appl. Phys. Lett.* **78** (2001) 733–735.
- 47 S. V. Andreev, B. R. Namofov, A. V. Koudinov, Y. G. Kusrayev, J. K. Furdyna. Spin depolarization of holes and lineshape of the Hanle effect in semiconductor nanostructures. *Phys. Rev. B* **80** (2009) 113301.
- 48 J. Fürst, H. Pascher, V. A. Abalmasov, T. S. Shamirzaev, K. S. Zhuravlev. Spin lifetime from Hanle-effect measurements in samples with InAs quantum dots embedded in different Al x Ga 1 x As matrices. *Semicond. Sci. Technol.* **20** (2005) 209.
- 49 B. Pal, Y. Masumoto. Spin relaxation in charge-tunable InP quantum dots. *Phys. Rev. B* **80** (2009) 125334.
- 50 Y. G. Kusrayev, B. R. Namofov, I. V. Sedova, S. V. Ivanov. Optically induced spin polarization and *g*-factor anisotropy of holes in CdSZnSe quantum dots. *Phys. Rev. B* **76** (2007) 153307.
- 51 G. Gélinas, A. Lanacer, R. Leonelli, R. A. Masut, P. J. Poole. Carrier thermal escape in families of InAs/InP self-assembled quantum dots. *Phys. Rev. B* **81** (2010) 235426.
- 52 H. Gotoh, H. Ando, H. Kamada, A. Chavez Pirson, J. Temmyo. Spin relaxation of excitons in zero-dimensional InGaAs quantum disks. *Appl. Phys. Lett.* **72** (1998) 1341–1343.
- 53 M. Paillard, X. Marie, P. Renucci, T. Amand, A. Jbeli, J. M. Gérard. Spin Relaxation Quenching in Semiconductor Quantum Dots. *Phys. Rev. Lett.* **86** (2001) 1634–1637.
- 54 L. M. Woods, T. L. Reinecke, Y. Lyanda Geller. Spin relaxation in quantum dots. *Phys. Rev. B* **66** (2002) 161318.
- 55 E. Tsitsishvili, R. v. Baltz, H. Kalt. Temperature dependence of polarization relaxation in semiconductor quantum dots. *Phys. Rev. B* **66** (2002) 161405.
- 56 B. Urbaszek, P.-F. Braun, T. Amand, O. Krebs, T. Belhadj, A. Lemaître, P. Voisin, X. Marie. Efficient dynamical nuclear polarization in quantum dots: Temperature dependence. *Phys. Rev. B* **76** (2007) 201301.
- 57 J. Fürst, H. Pascher, V. Shalygin, L. Vorobjev, D. Firsov, A. Tonkikh, N. Polyakov, Y. Samsonenko, G. Cirilin, V. Ustinov. Polarized photoluminescence of excitons in n-, p- and undoped InAs/GaAs quantum dots. *Int. J. Nanosci.* **6** (2007) 319–322.